COUPLING OF CHEMICAL KINETICS WITH COMPUTATIONAL FLUID DYNAMICS IN A THREE-DIMENSIONAL ENGINE MODEL

BY

HASSAN A. MAZI

THESIS

Submitted in partial fulfillment of the requirements
for the degree of Master of Science in Mechanical Engineering
in the Graduate College of the
University of Illinois at Urbana-Champaign, 2009

Urbana, Illinois

Advisor:

Professor Chia-Fon Lee

ABSTRACT

The role of computer modeling has grown recently to integrate itself as an inseparable tool to experimental studies for the optimization of automotive engines and the development of future fuels. Traditionally, computer models rely on simplified global reaction steps to simulate the combustion and pollutant formation inside the internal combustion engine. With the current interest in advanced combustion modes and injection strategies, this approach depends on arbitrary adjustment of model parameters that could reduce credibility of the predictions. The purpose of this study is to enhance the combustion model of KIVA, a computational fluid dynamics code, by coupling its fluid mechanics solution with detailed kinetic reactions solved by the chemistry solver, CHEMKIN. As a result, an engine-friendly reaction mechanism for n-heptane was selected to simulate diesel oxidation. Each cell in the computational domain is considered as a perfectly-stirred reactor which undergoes adiabatic constant-volume combustion. The model was applied to an ideally-prepared homogeneous-charge compression-ignition combustion (HCCI) and direct injection (DI) diesel combustion. Ignition and combustion results show that the code successfully simulates the premixed HCCI scenario when compared to traditional combustion models. Direct injection cases, on the other hand, do not offer a reliable prediction mainly due to the lack of turbulent-mixing model, inherent in the perfectly-stirred reactor formulation. In addition, the model is sensitive to intake conditions and experimental uncertainties which require implementation of enhanced predictive tools. It is recommended that future improvements consider turbulent-mixing effects as well as optimization techniques to accurately simulate actual in-cylinder process with reduced computational cost. Furthermore, the model requires the extension of existing fuel oxidation mechanisms to include pollutant formation kinetics for emission control studies.

To my Dearest;

Father and Mother

ACKNOWLEDGEMENT

First and foremost, praise is due to Allah, the Most Generous, for the continuous blessings that He bestows on me and my family. Truly, "*And my guidance cannot come except from Allah, in Him I put my trust and unto Him I repent*". Second, I would like to express my gratitude to my advisor, Professor Chia-Fon Lee for sharing his expertise and supporting me through hard times. I hope that I build on the wonderful experience at Illinois to become the excellent researcher every advisor proudly associates himself with. Third, deepest thanks go to my employer, the Saudi Arabian Oil Company, for the financial support and the continual scholarship. I thank Dr. Ted Kalivoda, of Aramco Services Company, who handled business matters and enabled full focus on academic progress. Many thanks go to the advisors and colleagues at the Graduate Automotive Technology Education (GATE) Center of Excellence for enriching my knowledge in the fields of engine research and fuel development, and for being a critical audience and a support group. I would also like to acknowledge the former and current members of my research group, without their contribution, computationally or experimentally, this work would be much harder. I specify Way Lee Cheng, for his continuous help in the Engine Modeling Lab, and Mike Leick, of the Ford Automotive Science & Technology Lab, for the experimental data. Last, but not least, I could not reach my academic and professional goals without the harmony and joy that my devoted wife, AlZahra, and our beloved sons, Haitham and Hatim, bring to my life.

TABLE OF CONTENTS

LIST OF FIGURES

LIST OF TABLES

CHAPTER 1: INTRODUCTION

1.1 Emission Regulations: A Driver to Engine Research

Since 1960, industrialized governments started to control pollution emitted from passenger and commercial automotive vehicles. These legislations are evolving tighter to the limit that what used to be measured in a gradual cylinder is now barely measured by a dropper [1]. Accordingly, a common trend in many relevant technical publications is to relate the "ever stringent" emission regulations to the motivation behind the work – which may also indicate that the development of the internal combustion (IC) engine is policy-driven.

Regulations in the United States, European Union and Japan target four types of pollutants, namely hydrocarbon (HC), carbon monoxide (CO), nitrogen oxides (NO_x), and particulate matter and soot (PM). The most stringent limits for these pollutants are 0.05, 0.5, 0.08, and 0.005 g/km, respectively, taking effect in the EU on 2014 [2]. Additionally, the EU has approved carbon dioxide (CO_2) limits which will take effect in 2010 [2] and aim to reduce it from 130 to 70 g/km between 2012 and 2025. This recent move not only challenges the very ideal operation of the IC engine, but it puts the development of alternative power-trains (e.g. hydrogen and electric) at advantage. As a result, the regulations paradigm has sparked renewed investment on the IC engine through the interplay of fuel research, engine development, as well as advancement in control and aftertreatment systems to reduce engine-out and tailpipe emissions.

Being the most challenging limits to be met, current research interests target engine-out NO_x and PM emissions using a combined approach that apply alternative fuels through multiple-injection strategies under advanced modes of combustion. The following discussion attempts to explain how engine design (injection and combustion characteristics) and fuel development could address the challenge of reducing NO_x and PM emissions to meet the unparalleled limits.

NO_x is formed under higher temperatures and in fuel-rich regions, while soot, a distinct by-product of diesel combustion, is formed under fuel-rich conditions [3]. It is possible to inject the fuel early on the cycle, such that the fuel-air mixture is lean, to control PM, but that will increase NO_x production due to high peak cylinder temperatures – giving rise to a paradox known as the NO_x-soot trade-off. One possibility for simultaneously minimizing both NO_x and PM emissions is to undergo a fuel-lean, low-temperature combustion. One drawback, however, of full reliance on this technique is power reduction since the emission reduction occurs at the expense of fuel consumption. As a result, a better approach to this problem may be to optimize fuel consumption by having multiple injection events that reduce PM and soot, but may slightly increase NO_x [4]. At that point, aftertreatment systems are used to capture the trapped pollutant using medium-to-high efficiency aftertreatment systems.

1.2 Research Motivation

In addition to addressing the problem through engine optimization, it might be possible to reduce the formation of pollutants at the source, i.e. the fuel. Accordingly, researchers are studying alternative fuels and novel fuel blends to understand the chemistry of fuel oxidation, pollutant formation and reduction. For instance, bio-derived fuels, such as biodiesel, which are receiving governmental support in the United States because they are renewable and are viewed to reduce dependence on foreign oil, are leading an enthusiastic research effort. Some of its disadvantages, however, is that pure biodiesel has lower heat capacity compared to diesel, and, inconclusively, produces higher NO_x emission.

To obtain a better answer for such an observation, engine researchers – through experiments and computational models – study fuel chemical kinetics and physical characteristics and their interaction inside the combustion chamber. It might escape the mind, but fuels as common as gasoline or diesel are complex mixtures of long-chain hydrocarbons which properties vary due to differences in crude quality and additives used. Similarly, biodiesel comes from different vegetable oils and animal fats, and therefore demands detailed

representation of the chemical and physical properties. As a result, researchers are relying on computer models to reduce the costs of experimental investigations and gain better understanding of phenomena inside the combustion chamber. A reliable computer code, therefore, models the detailed chemical and physical processes to predict the ignition, combustion and emission evolution and their interaction with the turbulent flow field.

1.3 Anticipated Contribution

This research builds a computer interface that integrates detailed chemistry with a computational fluid dynamics (CFD) code. It is an initial model in the sense that (1) it limits the study to fuel oxidation without implementation of pollutants kinetics, and (2) it does not implement all the currently-understood features described in the Literature Review Section. Specifically, the work in this thesis addresses the following areas:

- Evolution of CFD-detailed chemistry integration models,
- Optimization techniques to balance computational cost and accuracy,
- Pre-processing requirements for reaction mechanisms,
- Development of a coupled, fully-integrated CFD-chemistry model, and
- The number of species that could be limited to the fluid cycle.

1.4 Thesis Layout

The thesis starts by a literature review that further explains the problem, discusses how similar models are built and highlights important optimization techniques. Then, it is followed by an overview of the CFD and chemistry software used in the present work. After that, it describes the model development process, followed by discussion of the results, and concludes by offering recommendations for future work.

CHAPTER 2: LITERATURE REVIEW

In scientific computing, many simplifications and assumptions are made to the mathematical model such that it is readily implemented and computationally affordable. With the rapid development to computer processors and expansion of allowable memory, scientists and engineers are able to revisit some of the assumptions in effort to enhance the predictive capabilities of the model; a trend which is often observed in engine simulation tools. For this research, the goal is to shift from using multi-step global reactions to a manageable number of elementary reaction steps which governs the kinetics of fuel oxidization and pollutant formation. This chapter introduces some of the challenges associated with modeling advanced modes of combustion. After that, it goes on to explain the evolution of integrated CFD-chemistry models, their current development and the required computational optimization techniques for high fidelity simulations.

2.1 Emerging Combustion Modes

The spark-ignition (SI) and compression-ignition (CI) engines drive the two classes of automotive engines which are commonly referred to as gasoline and diesel engines, respectively. There are a number of distinct characteristics of each engine that controls ignition, combustion and resulting emissions. First, the ignition in an SI engine is triggered by a condensed electric charge which is timed to deliver a desired amount of power in a given load. On the other hand, the diesel is compressed in the CI engine and is ignited by controlling a series of parameters related to the injection event, such as the start-of-injection, injection duration, injection pressure, etc. Thus, the combustion of an SI engine is characterized by propagation of a flame that emerges from the kernel of hot gasses due to the spark power. The CI combustion, however, is more of a diffusion flame where the combustion occurs between the spray and surrounding mixture. Full reliance on conventional combustion modes yield high temperatures and subsequently high overall emissions which cannot meet future regulations. Thus, a number of alternative combustion modes are being studied.

The homogeneous-charge compression ignition (HCCI) combustion is a combustion mode, rather than an engine type, which capitalizes on the high efficiency and low NO_x and PM emissions inherent in CI and SI engines, respectively. The charge, i.e. air-fuel and residual gasses mixture, is self-ignited by compression producing a volumetric combustion that is unique to any other combustion mode. Furthermore, because HCCI could utilize either gasoline or diesel fuels, and due to its limited operating window, it is very common in research studies that a mixed-mode of combustion of HCCI is combined with SI or CI. The so-called homogeneous mixture is achieved by pre-mixing the fuel with air in the intake port (also called fumigation) or by direct injection of the fuel into the cylinder at an early stage to allow ample time for the mixture to become homogeneous [5]. Since the mixing time could be shorter, the term partially-mixed-charge compression ignition (PCCI) combustion is often used to highlight the inevitable inhomogeneity in the mixture. This combustion type is widely accepted to be kinetically-controlled which as a result puts simplified chemistry models at a disadvantage. Disadvantages of HCCI combustion include high HC and CO emissions, high peak pressures and heat release rates.

Another emerging combustion mode is the low-temperature combustion (LTC) which is a diesel combustion that includes some of the benefits of HCCI. While both LTC and HCCI utilize exhaust gas recirculation (EGR) to dilute and cool down the mixture, the term "low-temperature combustion" is often associated with the diesel stratified combustion (LTC) which differs in principal with HCCI combustion. Accordingly, the terms HCCI and LTC must not be used interchangeably. The diesel LTC relies on EGR (lower than amounts used in HCCI) to dilute the mixture, and multiple-injection events which control ignition and combustion.

The need for integration of detailed chemical kinetics arises because of the kinetics-controlled feature of HCCI and the low-temperature chemistry associated with spray combustion in LTC. Traditionally, global-step chemistry models (reviewed briefly in Section 3.2.3) assume full conversion of fuel into

products which effectively does not consider chemical kinetics and therefore unreliable emission prediction. In addition, such models are temperature-independent which gives room to arbitrary model parameter adjustments to "match" experimental pressure and heat release results.

2.2 Integration of Detailed Chemical Kinetics into CFD

Similar to the evolution of engine CFD codes, as a whole, the detailed chemistry integration with CFD has evolved in the same fashion progressing from simplified, single-zone, zero-dimensional models to more realistic physical and chemical sub-models in three dimension. One understanding, however, remained unchanged and that is the numerical study of detailed chemical kinetics with CFD is computationally expensive due to the extended size of the reaction mechanism. Consequently, this section describes the development of the CFD-chemistry models and addresses the importance of sub-grid turbulence consideration. Moreover, it covers crucial optimization techniques that should be implemented to reduce computational time while maintaining solution accuracy.

2.2.1 Basic Model based on Perfectly Stirred Reactor (PSR)

The simplest integrated model would be a single-zone model which represents the whole computational domain as one perfectly stirred reactor (PSR) with uniform temperature, pressure and composition distributions. Such approach is not adequate for engine simulations since it does not take into account gradients at different parts of the combustion chamber (such as the walls and piston bowl) and consequently does not predict emissions and burn rate correctly. Typical results, shown in Figure 2-2, demonstrate rapid heat release, and corresponding high peak pressures and fast burn rate which are usually over-prediction of experimental results.

Aceves et al [6] and [7] implemented one of the first CFD models that implement detailed chemistry beyond the single-zone model. In their work, the CFD-chemistry integration was sequential, meaning that the CFD and chemistry solutions were obtained in stages. First, the CFD code, KIVA, started

the simulation at inlet valve closing (IVC) until a point along the motoring curve (e.g 5° BTDC), where, presumably, no ignition or combustion had occurred. The initial mixture temperature (at IVC) was assumed to be uniform in the whole cylinder and initial values for swirl ratio and turbulence intensity were specified to account for the initial flow field. The computational mesh was two-dimensional with high local resolution to properly account for crevice flow and boundary layer at the wall.

After the CFD calculation reached its termination point, a transitional step prepared the grid for the chemistry calculation. The CFD computational domain, consisted of 160,000 cells, was transformed into 10 zones, shown in Figure 2-1, and was used as the new domain for the detailed chemistry solver HCT (stands for hydrodynamics, chemistry and transport [6]). As a result of this sequential approach, the two solutions are de-coupled since the high resolution CFD solution is lost in the one-way communication. The initial temperature for the multi-zone chemistry was calculated from the CFD temperature histories and passed to the detailed chemistry solver. The pressure was assumed constant for all zones and the volume change was computed due to piston movement, heat transfer and heat release. Furthermore, the zones did not interact with each other except in the case when combustion occurred in one zone causing its volume to expand, and consequently the volume of neighboring zones would compress. The HCT solver modeled the ignition of natural gas using the GRI mechanism (179 species in 1,125 reactions) which also includes NO_x kinetics.

Figure 2-2 shows improvement in predicted pressure traces from the multi-zone sequential code, compared to single-zone model, where the burn rate and peak pressures are within 10% of the experimental results. However, HC and CO emission predictions were under-predicted for all studied cases. The biggest advantage of this model is the reduced number of zones over which the detailed chemistry solver is subjected – which is a key optimization approach as will be discussed in Section 2.4.1. One disadvantage, however, of the sequential model is the loss of CFD data once the chemistry solver is called. The implications of

the de-coupling are two-fold; species transport is handicapped due to de-coupling of fluid dynamics and the model validity is limited to ideal HCCI simulations.

2.2.2 PSR with Turbulent-Mixing Effects

Kong and Reitz [8] proposed an enhanced model which couples the CFD and chemistry solutions for each cell in the domain at every time step. The thermodynamic state of each cell is shared between KIVA and CHEMKIN. KIVA supplies the initial species densities, pressure and temperature, while CHEMKIN, in return, calculates the change in species density and the heat release rate. The governing equations, according to [9], are given for a constant-volume adiabatic combustion as:

$$\frac{dY_k}{dt} = \frac{\dot{\omega}_k W_k}{\rho} \tag{2-1}$$

$$\frac{dT}{dt} = -\frac{1}{\rho\, \bar{c_v}} \sum_{k=1}^{K} \dot{\omega}_k W_k e_k \tag{2-2}$$

$$\dot{\rho}_k^{chem} = \rho \frac{dY_k}{dt} \tag{2-3}$$

$$\dot{Q}^{chem} = -\sum_{k=1}^{K} \frac{dY_k}{dt} \frac{\Delta h_{f\,k}^0}{W_k} \tag{2-4}$$

where,

Y_k:	mass fraction for species k
$\dot{\omega}_k$:	molar production rate for species k
W_k:	molecular weight for species k
ρ:	average cell density
$\bar{c_v}$:	cell averaged specific heat at constant volume
e_k:	specific internal energy for species k
$\dot{\rho}_k^{chem}$:	change in species density due to chemical reactions
$\dot{Q}^{chem}$:	heat release rate from all chemical reactions
$\Delta h_{f\,k}^0$:	molar heat of formation for species k

The source terms, given by the Equations (2-3) and (2-4) above, are those exchanged with KIVA. The constant-volume formulation shown above requires a small time step, usually on the order of 1 μs, which effectively restricts the fixes the volume of a given cell during the heat addition process.

This model improves the perfectly-stirred reactor (PSR) assumption by including sub-grid turbulent-mixing effects (it must be emphasized at this point that both models consider turbulent interactions on the large-scale through the k-ε model). Slightly modifying the notation in [8] for consistency, the molar production rate is equal to the change in species concentration and is written in terms of kinetic and turbulent time scales as:

$$\dot{\omega}_k = \frac{d[X_k]}{dt} = \frac{[X_k]^* - [X_k]}{\tau_{kin\,k} + \tau_{turb}} \tag{2-5}$$

where,

$[X_k]$:	species concentration
$[X_k]^*$:	equilibrium species concentration
$\tau_{kin\,k}$:	kinetic time scale for species k
τ_{turb}:	turbulent time scale

In the PSR formulation, as that by Aceves et al [6], the kinetically-controlled molar production rate is obtained from the chemistry solver. As a result, Equation (2-1) could be re-written in terms of the PSR solution, consistent with Equation (2-5) as:

$$\dot{\omega}_{k\,kin} = \frac{d[X_k]}{\tau_{kin\,k}} = \frac{\Delta[X_k]}{\Delta t} = \frac{[X_k]^n_{Chem} - [X_k]^n_{CFD}}{\Delta t} \tag{2-6}$$

where,

Δt:	hydrodynamic time step
subscript,	
n:	previous time step
superscripts,	
CFD:	solution before chemistry is called
Chem:	solution at end of chemistry call

If the sub-grid turbulent mixing effects are to be included, the change in species concentration is consequently given by:

$$[X_k]^{n+1} - [X_k]^n = \frac{\tau_{kin\,k}}{\tau_{kin\,k} + f\,\tau_{turb}} \Delta[X_k] \tag{2-7}$$

This expression, by Kong and Reitz [5], assumes that the fuel concentration at equilibrium is zero since the fuel will be converted to intermediate species soon after beginning of chemical reaction. Furthermore, it differs from (2-5) in that it

implements a combustion progress variable, f, defined below, which activates the turbulent mixing effects after the start of combustion.

$$f = \frac{1 - e^{r}}{0.632} \tag{2-8}$$

where,

r: ratio of current amount of products to total products of complete combustion

Note that the ranges of both r and f above range from 0 (i.e. combustion has not started) to 1 (complete combustion). In other words, before ignition occurs, the model is purely kinetically-controlled, but as soon products begin to form, the effects of turbulent mixing are taken into account.

The time scales in (2-7) are given as follows [8]:

$$\tau_{turb} = C\,\frac{k}{\varepsilon} \tag{2-9}$$

$$\tau_{kin} = \max(\tau_{kin\,fuel}, \tau_{kin\,CO}) \tag{2-10}$$

The turbulent timescale is proportional to the eddy turnover time, k/ε. As a result, the constant of proportionality, C, should depend on the selected turbulence model. For reference, suggested values are shown in Table 2-1 which may indicate the need for combustion mode and engine-specific adjustment. On the other hand, the kinetic timescale for all species is assumed to be equivalent to that of the fuel for simplicity. Thus, the subscript k is dropped. Furthermore, the maximum of the timescales for the fuel or CO, which exhibits a significant impact on heat release, is used as the rate limiting factor to avoid blowing up the term when fuel is consumed.

The turbulent-mixing model, [8], was validated against three experimental engines, however, for this limited discussion, only results from the Volvo converted-HCCI engine, specifications and operating conditions shown in Table 2-2, are considered. The piston head was flat to give a pancake combustion chamber. Pressure was supercharged and intake temperature was heated to ensure auto-ignition and combustion phasing, respectively. The engine was

fueled with natural gas which had a considerable amount of higher hydrocarbons. Hence, the natural gas reaction mechanism included heavier hydrocarbons up to n-butane and consisted of 211 species and 1,174 reactions. Because of the big size of the mechanism, a two-dimensional domain was used. The initial mixture temperature and composition was assumed to be uniform for all cells at the beginning of the simulation (i.e. at IVC).

The pressure and heat release results obtained with and without turbulent-mixing effects are shown in Figure 2-3. The peak pressure and main heat release are over-predicted with the perfectly-stirred reactor (PSR) model (i.e. kinetics-controlled model). This is due to the ideal homogeneity assumption which implies the existence of so-called hot-spots (throughout the whole domain) which auto-ignite simultaneously resulting in a rapid heat release evident by the slope of pressure rise. On the other hand, the addition of turbulent-mixing effects to the model enhances the peak pressures as well as the heat release on all three cases. The ignition timing agrees better in the boosted pressure cases than it does in the naturally aspirated case.

Overall, Kong and Reitz [8] concluded that the effects of turbulent mixing need be considered to provide better model comparison with experimental data. In addition, the use of a two-dimensional mesh is sufficient when the initial mixture is assumed to be homogeneous. A shift towards three-dimensional grid is necessary to resolve the spray dynamics for practical HCCI-like conditions. Lastly, the integrated CFD-chemistry model relies on an accurate reaction mechanism which parameters are unchanged for all engine cases.

2.2.3 Partially-Stirred Reactor (PaSR) Models

In the development of the turbulent-mixing effects model proposed by Kong and Reitz, [8], two assumptions were made. First, the fuel concentration at equilibrium is zero; and second, the kinetic time scale of all species is equal to that of the reference species. Hong et al, [10], argue that the first assumption leads to a relatively long kinetic time, while the second assumption, which

determines the transition from kinetic to turbulent combustion, is based on arbitrary selection of the reference species. As a result, a number of models such as Hong et al[11] and Golovitchev and Nordin [12], proposed models which model each computational cell as a partially-stirred reactor (PaSR).

Derived from the eddy dissipation concept (EDC), recently reviewed in [13], Golovitchev and Nordin [12] propose that a PaSR model is more appropriate to diesel combustion. A partially-stirred reaction divides the computational cell into two zones; (1) a reactive zone in which all reactions occur, and (2) a non-reactive zone. Golovitchev and Nordin [12] demonstrate this concept by Figure 2-4 which shows the change in concentration in two, parallel steps; I and II. In step I, the initial concentration at the cell level changes from c_0 to c as the mixture reacts. Simultaneously in step II, turbulence mixes the reactive mixture, c, and non-reactive mixture, c_0, resulting in an average concentration c_1. In the PSR model previously discussed, the change in species composition the model predicts is equivalent to the change from c_0 to c_1 which takes place within the numerical time-step, τ.

Similarly, the modified EDC model, Hong et al[11], represents the molecular mixing at the sub-grid level where reactions occur in a reaction zone or fine structure, illustrated by Figure 2-5. This model enhances Equations (2-1) and (2-2) by incorporating transient terms that account for the turbulence in the fine structure, making the model equally applicable to premixed or stratified combustion applications [11]. Because implementation of turbulent combustion effects is beyond the scope of this thesis, the reader is referred to the original literature for models adopting the PaSR approach; [10], [11] and [12].

2.3 Reaction Mechanisms

The most important input to the success of the integrated chemistry-CFD model is the kinetics mechanism which contains elementary reaction rate information, Equation (4-1), for a finite number of species and reactions. The size of the mechanism (i.e. the number of reactions and participating species)

depends on the molecule of interest and the range over which the mechanism is validated. Two terms are often used to describe the mechanism size; comprehensive and skeletal, but this notation is not based on a clearly-defined criteria. A *comprehensive* mechanism contains an extensive amount of reactions information and participating species which makes their application to engine simulations unpractical. A *skeletal* mechanism, on the other hand, includes significant reaction pathways that represent a comprehensive mechanism in a reduced, manageable size.

For the purpose of multidimensional engine modeling, the reaction mechanism sought after is essentially a skeletal mechanism of the fuel which has been reduced further to operating conditions of typical engine applications. Such mechanisms have been vigorously validated against experimental data at different pressures, equivalence ratios, as well as within the low- and high-temperature branches. Because diesel, for instance, is a very complex mixture of heavy hydrocarbon which detailed composition is granted to differ by supplier, a fuel surrogate (a relatively simpler, single molecule) is used to represent the real "pump" fuel. Successful studies at the Engine Research Center (ERC) of the University of Wisconsin-Madison have applied n-heptane as a surrogate for diesel, [14], while methyl butanoate as the surrogate for biodiesel, [15]. Throughout this study, the ERC n-heptane mechanism, [14], was used.

Three of the main key characteristics of hydrocarbon surrogates that must be exhibited regardless of size are (1) cool-flame region or two-stage heat release, (2) negative temperature coefficient (NTC) region, and (3) auto-ignition timing. The negative temperature coefficient region is a region where the ignition delay increases with increasing temperature. This trend is a common feature of heavy and long-chain hydrocarbon and is unlike the normal trend of lower ignition delay at increasing temperatures. During this region, the cool flame or two-stage combustion diminishes.

2.3.1 Pollutant Reaction Mechanisms and Models

One important feature of engine models is the ability to predict emissions with great accuracy. When detailed chemistry for fuel oxidation is implemented, kinetics of carbon monoxide (CO) and hydrocarbons (HC) are accordingly integrated. Similarly, the extended Zel'dovich mechanism provides a commonly accepted model for NO_x formation and oxidation which has been applied successfully to diesel engines. If more kinetic steps are desired, one could append nitrogen reactions from methane or natural gas mechanisms, such as the GRI mechanism, to the fuel oxidation mechanism. On the other hand, soot and particulate matter undergo a complex process that includes nucleation, surface growth and oxidation, and coagulation processes. Modeling of these processes might be much expensive than fuel oxidation, as a result, it is common that empirical models are implemented in CFD simulations (briefly discussed in Section 3.2.3). Most recently, an engine-friendly multi-step model, developed by Hong et al [11], was integrated with a skeletal n-heptane mechanism. The model was validated with shock tube studies and was shown to be valid over an extended engine operating window.

2.4 Optimization Techniques

From the previous discussion, the number of ODEs in the system of interest is equal to the number of species plus two; i.e. those formed by Equations (2-2) to (2-4) above. Further, when the model is applied to direct-injection diesel simulations (requires high resolution to resolve spray dynamics) the associated computational cost increases drastically due to the increase in frequency of chemistry calculations. As a result, the integration of detailed chemical kinetics into CFD becomes indeed a very costly process even with the latest computers. Thus, it is crucial that the base model be optimized such that the high-fidelity model could be used as a parametric study tool.

There are at least three areas of optimization that have been studied and published in the literature and they form a triangle that greatly reduces the

computation time while having small impact on solution accuracy. Since the solution time depends on the number of ODEs, or reactions involved, the first optimization approach to the baseline model is to reduce the size of the reaction mechanism. This could be achieved either by further reduction of a skeletal mechanism and validation under engine-specific conditions, or by on-the-fly mechanism reductions (both approaches not within the scope of the thesis). Secondly, since the coupled model loops over all the cells in the domain, the computational time could be reduced if the chemistry solver has a lower-resolution. Hence, the size of CHEMKIN-based grid is reduced using multi-zoning or multi-grid techniques. The third area of optimization is the utilization of numerical analysis to develop semi-implicit solvers and parallel-processor execution of the code. The following section discusses these approaches.

2.4.1 Coupled Multi-Zone Model

Because a fully resolved CFD-chemistry model is expensive, techniques must be devised to reduce the computation cost even for the simplest reaction mechanisms. One remarkable contribution in this area is the work of Babajimopoulos et al [16] which aims to reduce the computation time without sacrificing solution accuracy by developing a coupled multi-zone model. Referring back to Equations (2-1) and (2-2) above, the chemistry solution is dependent on temperature, pressure and species composition of a given space. In other words, the volume of such space, or cell, is not important as long as the cell is represented by a similar thermodynamic state. This analysis promoted the idea of a multi-zone model where a set of parameters, temperature and a composition indicator, are computed for each cell. Cells of similar identities, according to the criteria selected, are then grouped into zones. As such, the chemistry calculations loop over zones, instead of cells, and results in CPU time savings as high as ten [16].

The thermodynamic state at each cell could be described by the pressure, temperature and composition. Pressure gradients are very small in HCCI and DI applications due to the low Mach number flows making it an unsuitable

grouping measure. The selection of temperature, on the other hand, as a zoning criterion is crucial due to dependence of reaction rates on temperature (and correspondingly ignition timing). The transient composition stratification parameter, on the other hand, is not. Babajimopoulos et al [16] investigated a number of parameters such as a global equivalence ratio, Φ (reduces to conventional definition), actual-to-stoichiometric fuel-O_2 equivalence ratio, Φ^*, and a progress equivalence ratio, φ, which is defined for a general fuel $C_H H_y O_z$ as:

$$\varphi = \frac{ch - z' C^{\#}_{-CO_2}}{O^{\#}_{-CO_2-H_2O} - z' C^{\#}_{-CO_2}} \tag{2-11}$$

$$ch = 2C^{\#}_{-CO_2} + 0.5H^{\#}_{-H_2O} \tag{2-12}$$

where,

z':	ratio of oxygen atoms to carbon, $z' = z/x$
ch:	number of carbon and hydrogen atoms, excluding contribution of complete combustion products (i.e. H_2O and CO_2)
superscript,	
#:	the number of atoms for each element
subscript,	less contribution of complete-combustion species to total count

These equivalence ratios, were calculated using a variable-volume reactor code based on CHEMKIN, and their evolution is shown in Figure 2-2. The global equivalence ratio, Φ, was kept constant throughout the cycle at 0.4, and replicated accordingly in the figure. Meanwhile, fuel-O_2 equivalence ratio, Φ^*, especially for higher hydrocarbons (i.e. iso-octane), starts to drop much before the main heat release since elementary reaction steps breaks it down to smaller hydrocarbons and radicals. The figure demonstrates, however, that the progress equivalence ratio, φ, corresponds well with the temperature profile (and main heat release) since it takes into account H_2O and CO_2 – which contribute to the main heat release. Accordingly, Babajimopoulos et al [16] grouped the CFD solution into a finite number of chemistry zones (100 in the present study) according to the $T - \varphi$ criteria. As a result, the aforementioned global cell zoning or grouping technique provides a reduced chemistry domain which is less computationally intensive yet represents the key features of the CFD domain.

In order to maintain the coupling of the CFD and detailed chemistry solutions, a reverse process, called re-mapping, is necessary. A simple approach utilizes an average remapping method where the mean value of a given parameter in a zone is returned to each cell – which would likely introduce numerical diffusion. Therefore, Babajimopoulos et al [16] proposed an enhanced re-mapping method based on conservation of the number of atoms (for all elements) in a zone and its comprised cells. Using the example of carbon atoms balance, the re-mapping is performed as follows:

$$m_k^{cell} = \frac{ch^{cell}}{ch^{zone}} m_k^{zone} \tag{2-13}$$

$$C_{cell}^{\#} = \sum_k \frac{m_k^{cell}}{M_k} c_k + \frac{m_{CO_2}^{cell}}{M_{CO_2}} \tag{2-14}$$

where,

m:	mass of species k (in a given cell or zone)
M:	species molecular weight
c:	number of carbon atoms in species k

Similarly, the same procedure is applied for carbon and hydrogen. Lastly, the number of nitrogen atoms in a cell is adjusted to match the original cell contribution. Figure 2-7 shows a comparison of the evolution of mass fractions of selected species (using methane as fuel) across the engine cycle as developed by [16]. It can be seen clearly that the "improved re-mapping technique" (i.e. discussed herein) provides a significant agreement with the full resolution chemistry solution especially as the chemistry becomes frozen. The average re-mapping method over-predicts CO_2 and severely under-predicts NO due to the under-estimated cell temperatures.

2.4.2 Adaptive Multi-Grid Chemistry Model

Shi et al [17] built on the model of [16] to develop a technique called adaptive multi-grid chemistry (AMC). The model differs from the global grouping technique of Babajimopoulos et al [16] by adding and adaptive spatial criteria for the zoning and re-mapping schemes, which increases model applicability to stratified DI simulations. In the global grouping method, it might be possible

that a number of scattered cells have the same progress ratio but that does not guarantee them having similar species mass fractions. In response to this problem, Shi et al [17] proposed that (1) the grouping be based on local, rather than global, conditions, and (2) the temperature standard deviation would determine the adaptive span of local uniformity. Thus, the temperature inhomogeneity is introduced:

$$\sigma_T = \sqrt{\frac{1}{n-1}\sum_{i=1}^{n}(T_i - \bar{T})^2} \tag{2-15}$$

where,

n: number of cells
T_i: cell temperature
$\bar{T}$: average cylinder temperature

Accordingly, cells which fall below a pre-specified temperature inhomogeneity or progress equivalence ratio thresholds are grouped together. The grouping could be up to four neighboring cells for a 2D mesh, as illustrated in Figure 2-10. The remapping is achieved by the same gradient-preserving technique proposed by [16]. The simulated pressure and heat release matched the results from the full chemistry solver yet the time savings were up to 10 times in HCCI applications and 2-3 times in DI combustion [17].

2.4.3 Semi-Implicit Solver

The non-linear ODE system of equation describing the chemical kinetic problem is classified as stiff, meaning there exists a range of time scales associated with the production or destruction of each species. As a result, the problem time-step is restricted in proportion to the smallest timescale in order increase solution stability. Consequently, the computation time is increased. Many researchers rely on the implicit ODEPACK, e.g. VODE [18], developed by Los Alamos National Laboratory, to solve the problem using a small time step, usually in the order of 1 μs. Others use the standard semi-implicit chemistry solver in KIVA [19] to solve the problem at hydrodynamic time steps (usually

much larger 1 μs), but the total number of reactions is limited due to loss of solution accuracy resulting from the stiff elementary steps.

One exception is presented by Liang et al [20] where a semi-implicit non-iterative method was developed. They developed a finite-difference scheme, up to third-order accurate, to solve the production rate, $\dot{\omega}_k$, of Equation (2-1) as:

$$\dot{\omega}_{k_i} = (v''_{ki} - v'_{ki})\, q_i \tag{2-16}$$

$$q_i = k_{f_i} \prod_{k=1}^{K} [X_k]^{v'_{ki}} - k_{b_i} \prod_{k=1}^{K} [X_k]^{v''_{ki}} \tag{2-17}$$

$$\dot{\omega}_k = \frac{d[X_k]}{dt} = f_k([X_l]) = f_k^+([X_l]) - f_k^-([X_l]) \tag{2-18}$$

where,

f_k: a short-hand notation for expanded terms in Equations (2-16) and (2-17)

superscript,

$+$: the strictly positive contribution of the overall source term, f_k

$-$: the strictly negative contribution of the overall source term, f_k

The finite-difference equivalent for Equation (2-18) is:

$$\frac{d[X_k]}{dt} = \frac{[X_k]^{n+1} - [X_k]^n}{\Delta t} = F_k^+([X_l]^n) - F_k^-([X_l]^n) \tag{2-19}$$

The standard KIVA chemistry solver [19] solves the above expression by introducing a damping coefficient that maintains solution stability as:

$$\frac{[X_k]^{n+1} - [X_k]^n}{\Delta t} = \frac{F_k^+([X_l]^n) - F_k^-([X_l]^n)}{1 + \frac{F_k^-([X_l]^n)\,\Delta t}{[X_k]^n}} \tag{2-20}$$

Thus, the new concentration is prevented from being driven negative since the denominator of (2-20) is always positive for all values of Δt. However, an inaccuracy is introduced in this scheme which is based on multiplying the new concentration from (2-19) by the factor, $[X_k]^{n+1}/[X_k]^n$, which equals unity to first-order. As a result, Liang et al [20] incorporated a predicted concentration ratio term that increases the solution accuracy, as shown in (2-21). In addition to the above, a sort algorithm and a sub-cycling scheme were implemented to reduce computation time, but that is not discussed here.

$$\frac{[X_k]^{n+1} - [X_k]^n}{\Delta t} = \frac{F_k^+([X_l]^n) - F_k^-([X_l]^n)}{1 + \frac{1}{[X_k]^n} \frac{\{F_k^-([X_l]^n)\,\Delta t\}^2}{[X_k]^n + \Delta t \cdot \{F_k^+([X_l]^n) + F_k^-([X_l]^n)\}}} \tag{2-21}$$

The results from this study for Scheme I, i.e. Equation (2-20), using the ERC mechanism show good agreement, as depicted in Figure 2-8, with experiment results except for late injection cases (SOI = +5 ATDC) which represent extreme conditions near the misfire limit of the engine. In such a case, both CHEMKIN solver and Scheme I predicted an earlier ignition by 7-8 degrees. Scheme II, implemented with the MIT mechanism, on the other hand, given by Equation (2-21) and shown in Figure 2-9, provide enhanced pressure traces to all simulated cases, using both the CHEMKIN and Scheme II solvers. It must be noted, however, that solution of the solver is sensitive to the reaction mechanism selected. The computation time using both semi-implicit schemes was reported to be 50-70% faster than the CHEMKIN solver. Although higher order discretization was used for Equations (2-20) and (2-21) above, there were no significant time savings reported over the first-order formulation.

2.4.4 Parallel Processing

One last optimization numerical approach that speeds-up the integrated chemistry calculations is parallel processing where the computational domain is divided into a number of sub-domains according to the number of available computer processors or CPUs. Each processor, as a result, shares the burden of the computation and loops concurrently over the assigned sub-domain cells. While there are successful attempts to parallelize the whole KIVA code, most recently [21], a common approach is to limit the parallelization to sub-models that consume most of the CPU time, such as the detailed chemistry interface, as reported by [22] and [23].

There are two standards or architectures for parallelism; shared- and distributed-memory. In the distributed memory architecture, standardized as Message-Passing Interface (MPI), each processor has an exclusive memory access. On the other hand, as the name implies, each processor shares access to

the centralized system memory, using OpenMP shared-memory compiler directives. As a general implementation note, OpenMP is viewed to be easier to program and allows partial or incremental code parallelization making it suitable for multi-core engineering workstations. Conversely, MPI is harder to implement and requires more computer resources – yet has the flexible feature to be run in a shared- or distributed-memory mode.

Ali et al [22] profiled the performance of KIVA-CHEMKIN code, based on Kong and Reitz [8], using SpeedShop on a SGI ORIGIN 2000 workstation. The study determined that the chemistry interface subroutine consumes more than 90% of the total computational time using a reaction mechanism consisting of 40 species and 165 reactions. To be specific, the detailed chemistry calculations accounted for 91% of 2D simulation (with 256 cells) and 98% of a 60°-sector (5,260 cells). Consequently, Ali et al [22], justified limiting KIVA parallelization to the detailed chemistry interface due to its domination to total computer time.

In theory, the speed-up factor, S – not considering CPU communication cost – is described by Amdahl's relationship as:

$$S = \frac{1}{(1-F) + \frac{F}{N}} \tag{2-22}$$

where,

F: portion of the code to be parallelized, and
N: number of processors.

Ali et al [22] plotted Equation (2-1) against the results of KIVA-CHEMKIN parallelization using both of MPI and OpenMP standards. As shown in Figure 2-11, under OpenMP and shared-memory MPI, the code is two times faster if executed with four processors. The study, therefore, suggested that OpenMP offers speed-up factors closer to the theoretical limit than shared-memory MPI does, since the improved performance of OpenMP increases monotonically with the number of species.

The KIVA-CHEMKIN parallelization of Ali et al [22] was based on even domain decomposition, where the computational domain is distributed evenly to

the number of processors. In other words, the load balancing strategy did not consider the variation in solution time due to the stiffy ODE problem based on the local conditions, e.g. mixture inhomogeneity. Thus, the parallelization method is not optimized, for a given time step, because the time spent at each processor would greatly be impacted by the number of CHEMKIN-active cells. In response, Shi et al [23] improved the load balancing scheme by distributing the domain by the number of cells which will be called by CHEMKIN. Most notably, the work of Shi et al [23], illustrates that combination of optimization methods, such as those described earlier, is crucial to striking a balance between the detailed physical and chemical sub-models and the associated computer cost.

2.5 Tables

	Combustion Mode [Reference]	
Turb. Model	DI [5]	HCCI [24]
Standard k-ε	---	0.142
RNG k-ε	0.020	0.100

Table 2-1: Suggested values for turbulent time scale model constant per [5] and [24].

Engine Specification	Volvo TD 100 Series Diesel Bore x Stroke: 120.65 x 140 mm Conn. Rod Length: 260 mm Displacement Vol: 1600 c.c. Compression Ratio: 19 Intake Valve Closure: 13 ABDC Speed: 1000 rpm		
Fuel— Natural Gas	Composition	Vol. %	Mass %
	Methane	91.1	81.0
	Ethane	4.7	7.9
	Propane	1.7	4.2
	n-Butane	1.4	4.7
	Nitrogen	0.6	0.9
	CO_2	0.5	1.2
Boost Pressure	0 bar	1 bar	2 bar
Intake Temperature	151 C	79 C	50 C
ϕ	0.379	0.292	0.260

Table 2-2: Volvo Converted-HCCI Engine Specification used in [8].

2.6 Figures

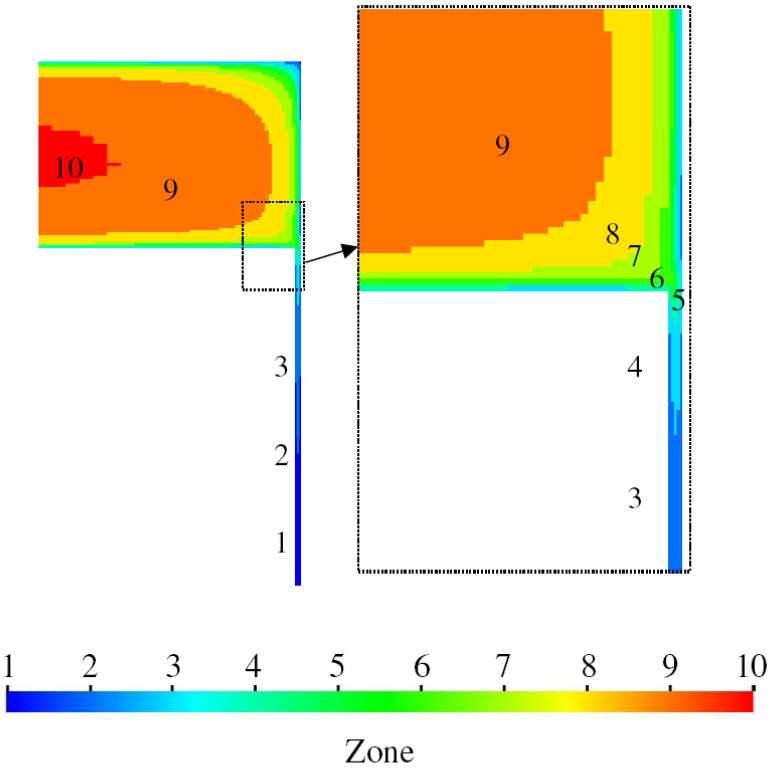

Figure 2-1: Graphical representation of the 10 zones in the computational domain used in [6] with a close-up on the crevice region zones.

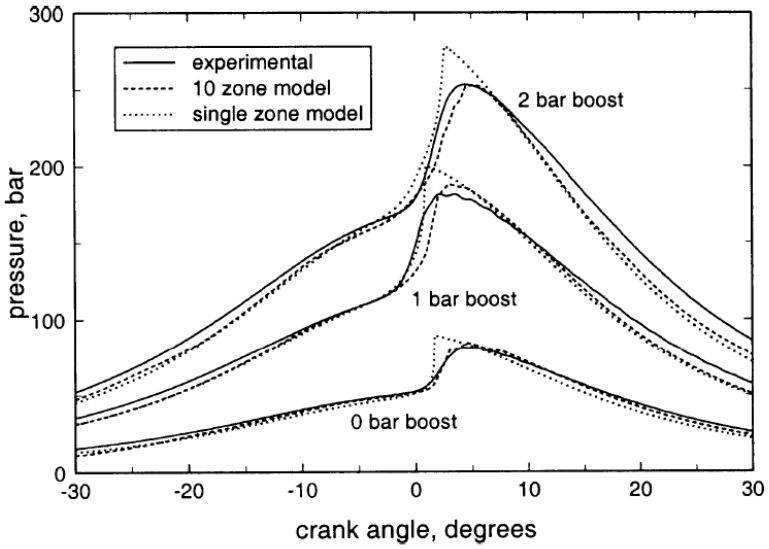

Figure 2-2: Comparison of experimental and computational pressure traces using a sequential (de-coupled) single- and multi-zone CFD-chemistry model [6]. Solid lines are experimental curves, dotted lines are single-zone computations, while dashed lines correspond to 10-zone model predictions.

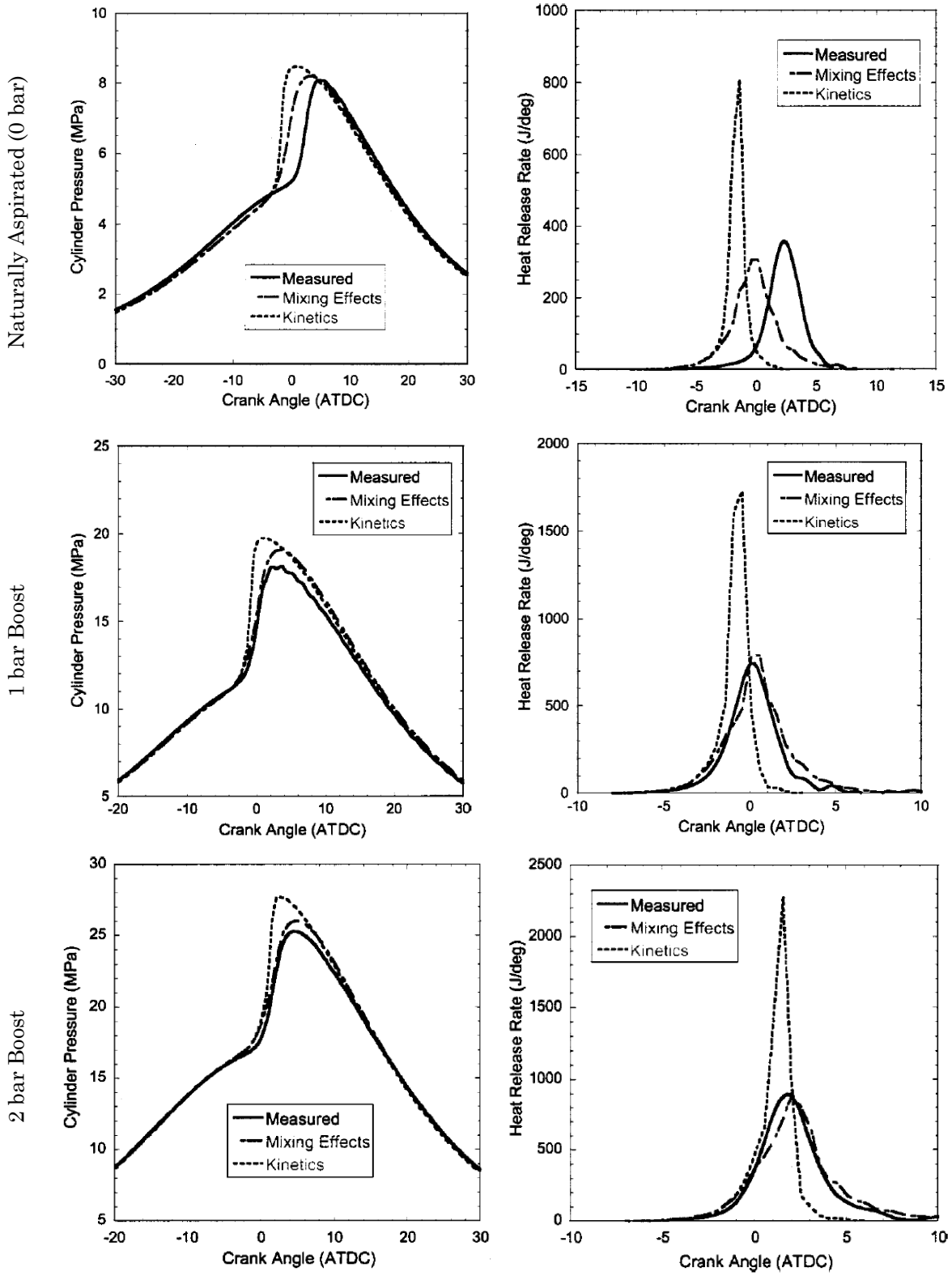

Figure 2-3: Pressure traces (left) and heat release rates (right) for Volvo Converted-HCCI Engine for naturally aspirated and two boost pressures conditions [8]. Solid lines are experimental curves, dotted lines are results of purely kinetic predictions, whereas the dashed lines depict the turbulent mixing solution.

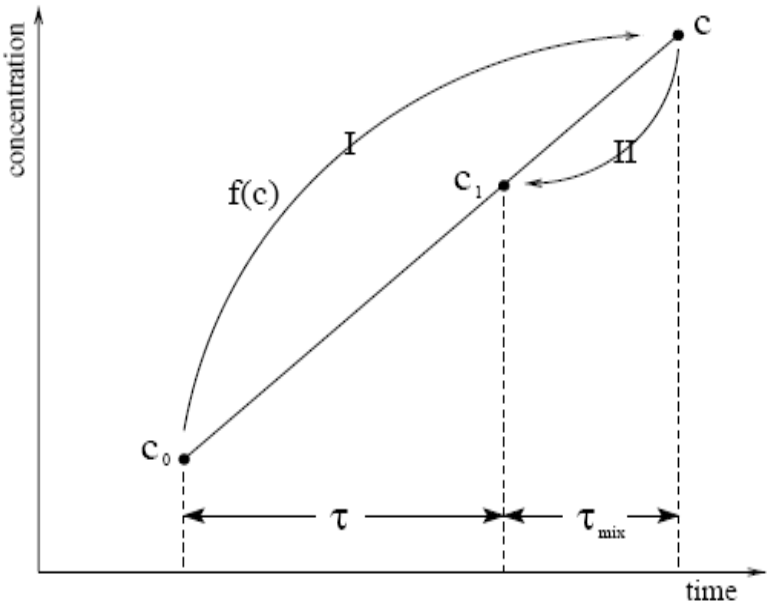

Figure 2-4: The PSR rate balance chart [12].

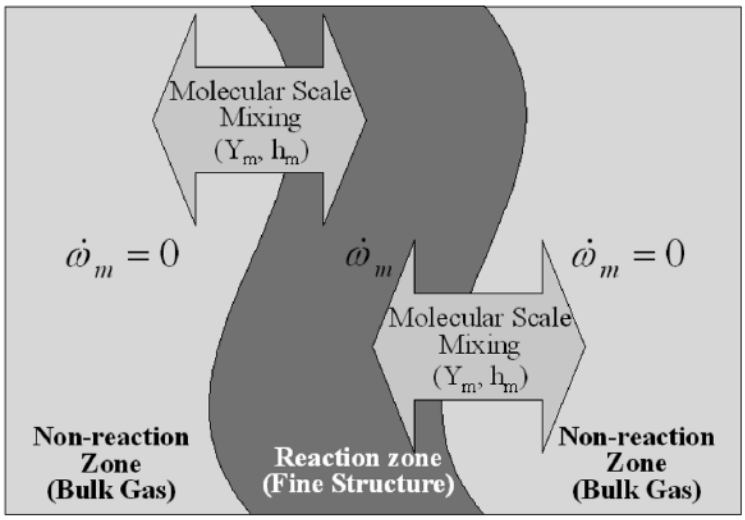

Figure 2-5: Schematic of the computational cell based on the modified EDC model [11].

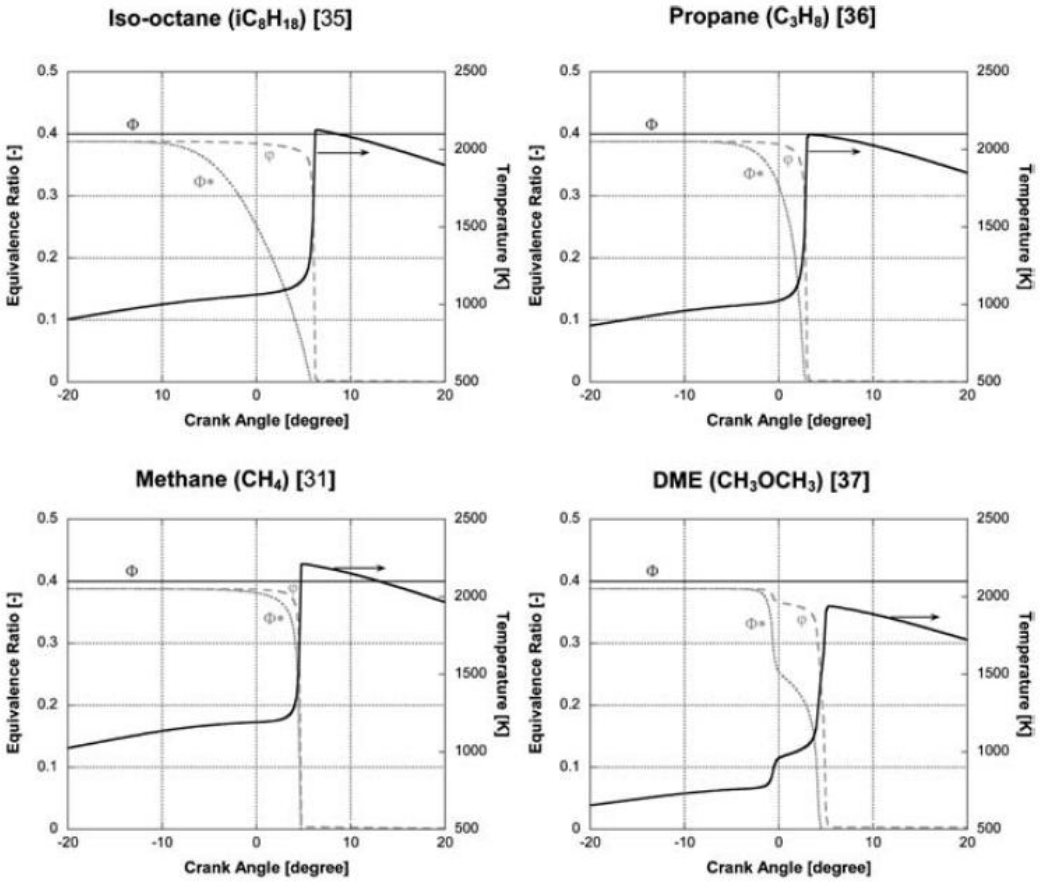

Figure 2-6: Evolution of different equivalence ratios used by [16] as a composition zoning criterion for four selected fuels with an initial global equivalence ratio of Φ = 0.4 and 5% EGR.
Note that the bracket (next to the fuel name) represents the reference to the reaction mechanism in [16].

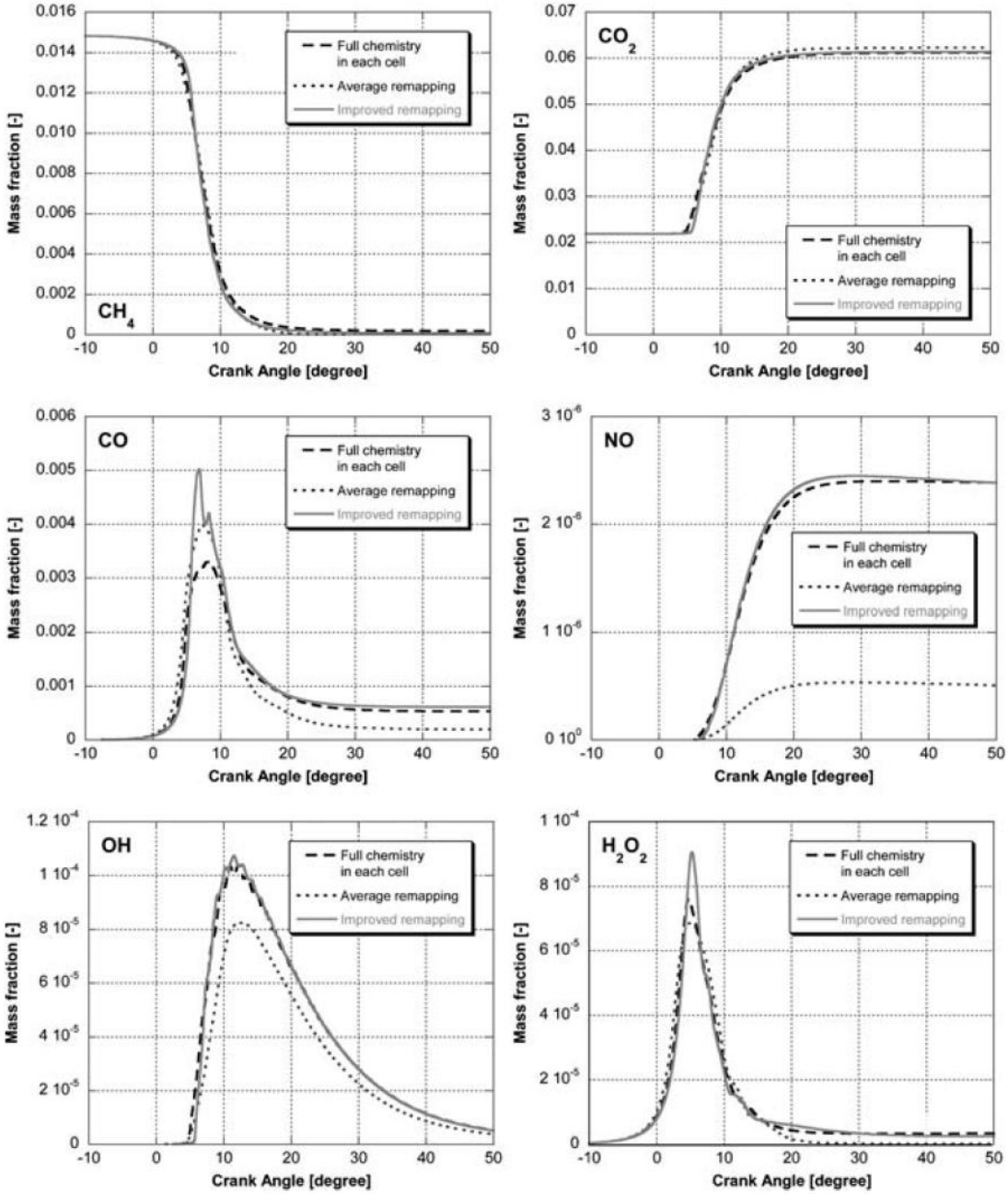

Fig. 10 Comparison of the evolution of the mass fraction of selected species using the multi-zone model with the two different remapping options (average and improved) against the detailed solution

Figure 2-7: Comparison of the evolution of the mass fraction for of selected species using two re-mapping techniques to couple the CFD-chemistry model[16]. Earlier discussion was limited to the development of the "improved re-mapping technique".

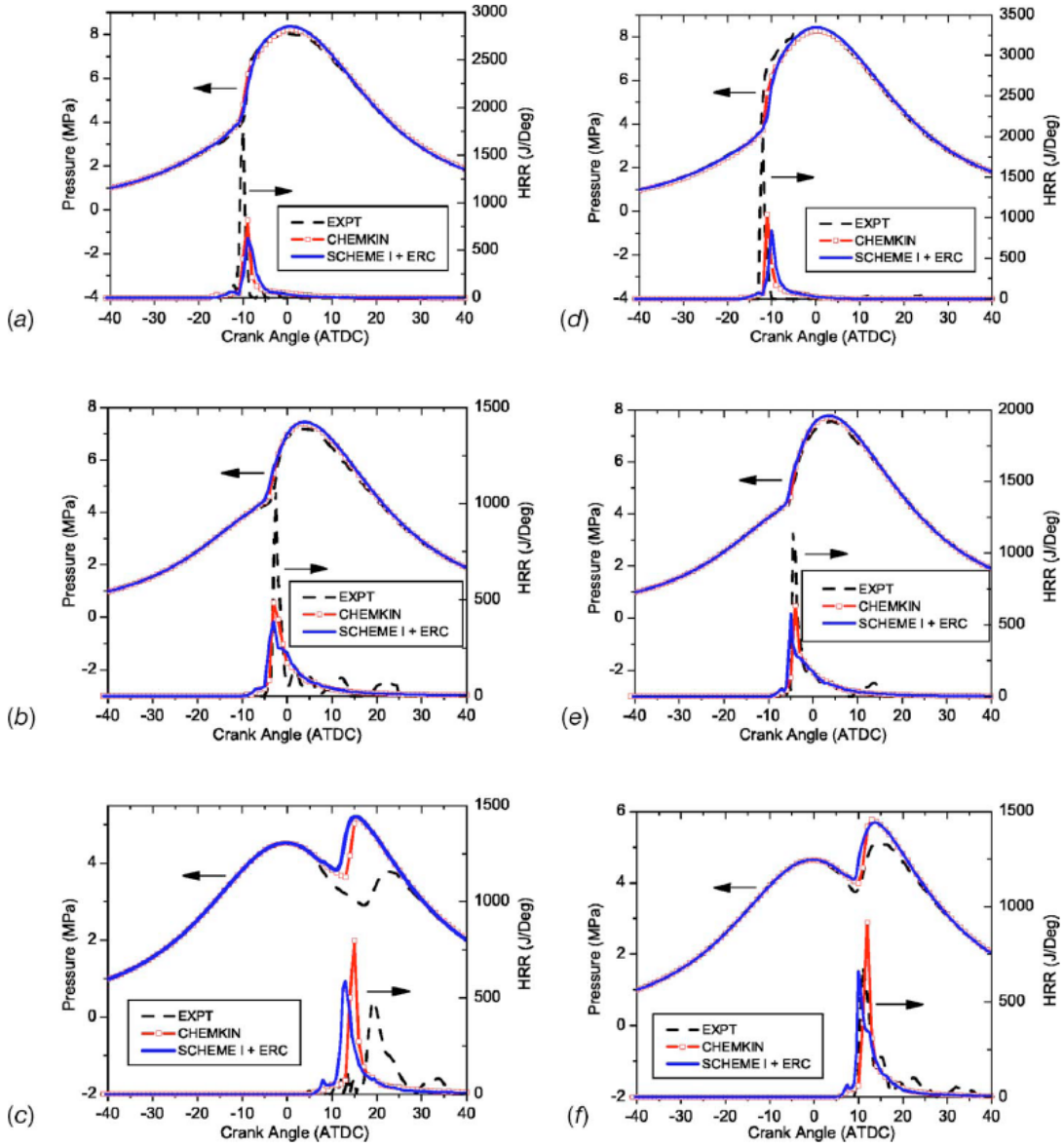

Figure 2-8: Comparison of pressure and heat release rate solutions using CHEMKIN and Semi-Implicit Scheme I solvers (ERC n-heptane reaction mechanism) [20] (a) SOI = -20 ATDC, 44% EGR. (b) SOI = -10 ATDC, 44% EGR. (c) SOI = +5 ATDC, 44% EGR. (d) SOI = -20 ATDC, 8% EGR. (e) SOI = -10 ATDC, 8% EGR. (f) SOI = +5 ATDC, 8% EGR.

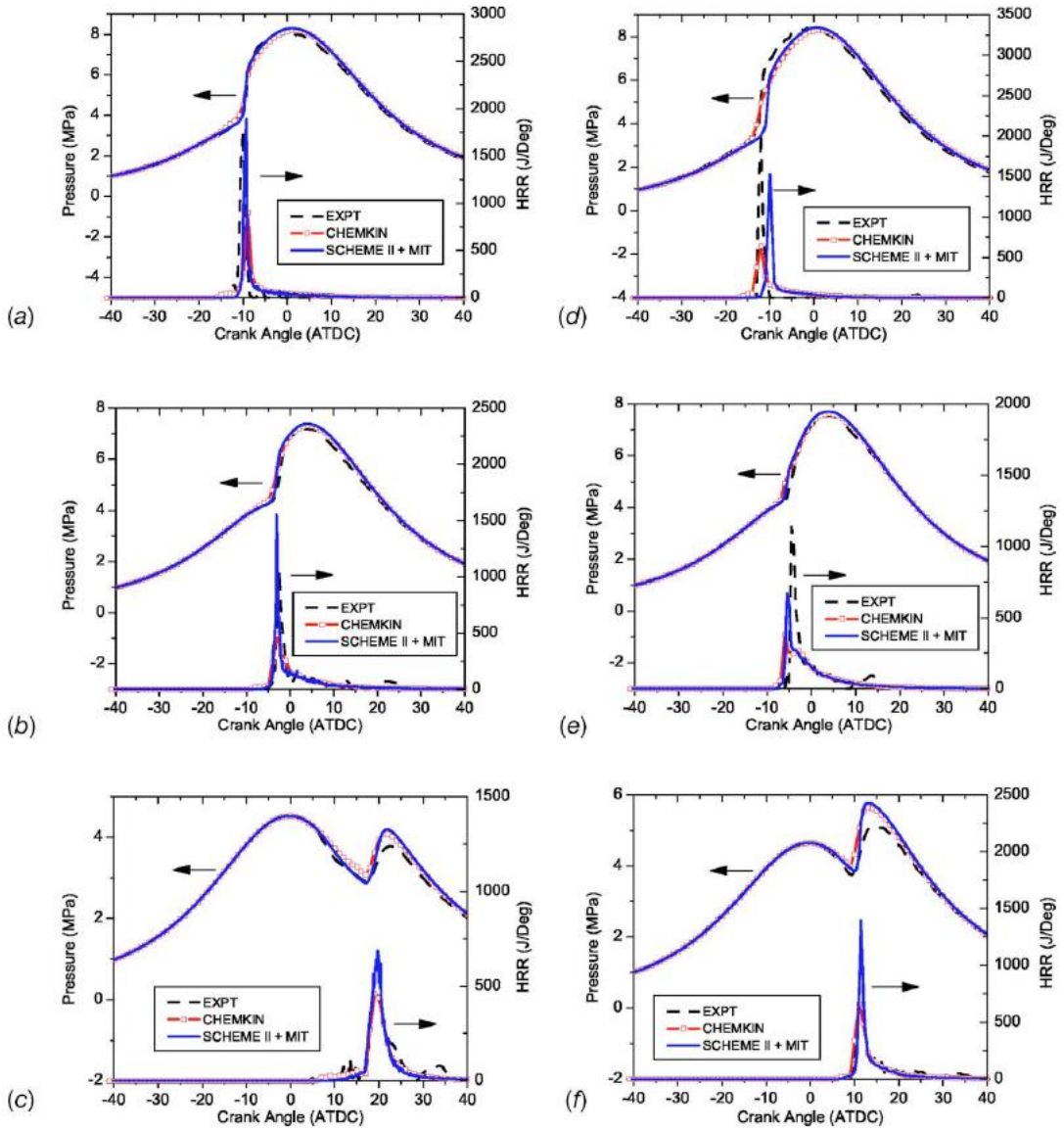

Figure 2-9: Comparison of pressure and heat release rate solutions using CHEMKIN and Semi-Implicit Scheme II solvers (MIT PRF reaction mechanism) [20] (a) SOI = -20 ATDC, 44% EGR. (b) SOI = -10 ATDC, 44% EGR. (c) SOI = +5 ATDC, 44% EGR. (d) SOI = -20 ATDC, 8% EGR. (e) SOI = -10 ATDC, 8% EGR. (f) SOI = +5 ATDC, 8% EGR.

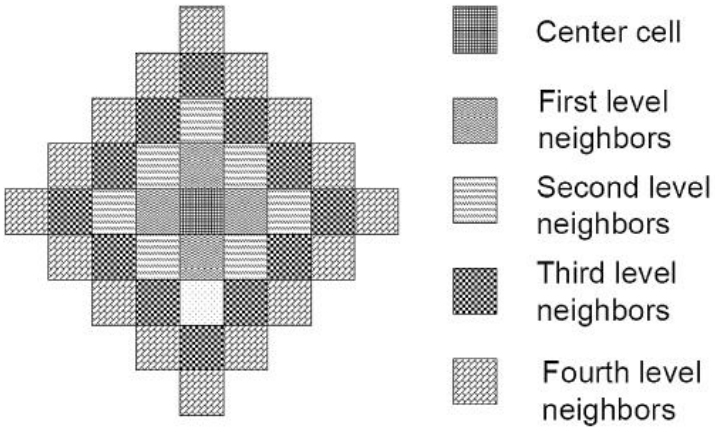

Figure 2-10: Adaptive multi-grid mapping showing up to four neighbors in a 2D mesh [17]

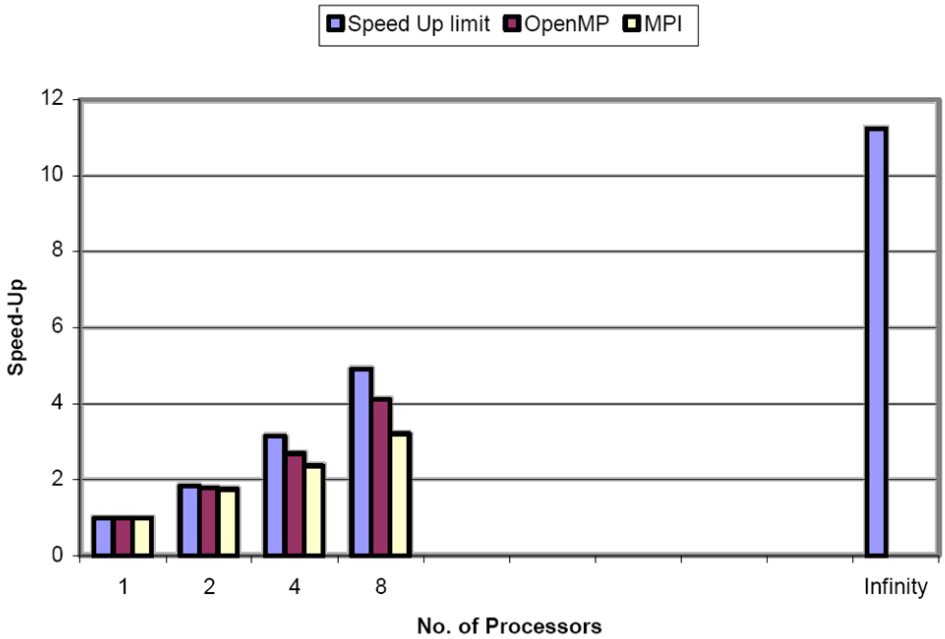

Figure 2-11: Comparison of speed-up obtained using OpenMP and MPI in comparison with Amdahl's law theoretical speed-up factor [22]
Three bins for the speed-up factor are shown per number of processors. The left bin corresponds to the theoretical limit, the middle to OpenMP parallelization, while the right column corresponds to MPI.

CHAPTER 3: THE KIVA CODE

The main objective of this thesis is to integrate detailed chemical kinetics into fluid dynamics software for better representation of the actual chemistry and physics inside the internal combustion engine. The computational fluid dynamics (CFD) code used for this study is KIVA which is developed by Los Alamos National Laboratory (LANL) and is customized by past researchers at the University of Illinois. The chemistry solver, on the other hand, was originally developed by Sandia National Laboratories [25] but is currently commercialized through Reaction Design. This chapter is dedicated to introducing the evolution of KIVA and is followed by the development of a user-defined Application Programming Interface (API) for CHEMKIN.

3.1 General Overview of KIVA

The KIVA family of Fortran codes evolved from the early '80s [19] to this day [26] establishing itself as a widely adopted design and research tool for complex reactive flow applications. Its success might be largely attributed to its open-source structure which allows the user to improve the physical representation of the sub-models as more insights are gained from experiments. Note that although KIVA could model a wide range of applications, the following discussion will be limited to internal combustion engine applications.

KIVA calculates the transient thermal and physical process inside a reactive domain and has the capacity to model liquid spray injection, droplet breakup and evaporation, gas-liquid charge mixing, ignition and combustion processes as well as heat transfer. KIVA employs the arbitrary Lagrangian-Eularian (ALE) method [27] to solve the governing equations and couples the solution of sub-models using the operator splitting approach. This approach makes it possible to incrementally add the contributions of change in species densities, for instance, due to piston movement, phase-change or combustion. As such, KIVA is centralized in a main program that calls other sub-models which in turn describe the different processes in the computational domain as they take place in time.

This computational domain, or grid, is composed of a number of cells, or finite volumes, which the ALE method requires to apply the governing equations. KIVA marches in time to solve the governing equations by sweeping over all cells in the domain, which increases the computational cost with the complexity and size of the domain.

The equations of motion for the unsteady, turbulent and chemically reactive flow are governed by the conservation of mass, momentum and energy:

$$\frac{\partial \rho_m}{\partial t} + \nabla \cdot (\rho_m \boldsymbol{u}) = \nabla \cdot \left[\rho\, \mathcal{D}\, \nabla \left(\frac{\rho_m}{\rho}\right)\right] + \dot{\rho}_m^c + \dot{\rho}^s\, \delta_{m1}$$
$$\frac{\partial \rho}{\partial t} + \nabla \cdot (\rho \boldsymbol{u}) = \dot{\rho}^s \tag{3-1}$$

$$\frac{\partial (\rho \boldsymbol{u})}{\partial t} + \nabla \cdot (\rho \boldsymbol{u}\boldsymbol{u}) = -\frac{1}{a^2}\nabla p - A_0 \nabla \left(\frac{2}{3}\rho k\right) + \nabla \cdot \sigma + \boldsymbol{F}^s + \rho \boldsymbol{g} \tag{3-2}$$

$$\frac{\partial (\rho I)}{\partial t} + \nabla \cdot (\rho \boldsymbol{u} I) = -p \nabla \cdot \boldsymbol{u} + (1 - A_0)\sigma : \nabla \boldsymbol{u} - \nabla \cdot \boldsymbol{J} + A_0 \rho \varepsilon + \dot{Q}^c + \dot{Q}^s \tag{3-3}$$

where,

ρ:	mass density
t:	time
$\boldsymbol{u}$:	fluid velocity vector
$\mathcal{D}$:	mass diffusion coefficient from Fick's law of binary diffusion
δ:	Dirac delta function
a:	dimensionless number used for low Mach number flows
p:	fluid pressure
σ:	viscous stress tensor
A_0:	flow regime flag, laminar (0), or (1) for turbulence models
$\boldsymbol{F}$:	rate of momentum gain per unit volume
$\boldsymbol{g}$:	specific body force, assumed constant
I:	specific internal energy, excluding chemical energy contribution
$\boldsymbol{J}$:	heat flux vector that sums heat conduction and enthalpy diffusion
k:	turbulent kinetic energy
ε:	turbulent dissipation rate

subscripts,

m:	species that compose the mixture (note change in notation)

superscripts,

c:	chemistry source/sink terms
s:	spray contribution, where fuel is assumed to be the first species

In addition, turbulent flows could be modeled using the k-ε equations:

$$\frac{\partial (\rho k)}{\partial t} + \nabla \cdot (\rho \boldsymbol{u} k) = -\frac{2}{3}\rho k \nabla \cdot \sigma + \sigma : \nabla \boldsymbol{u} + \nabla \cdot \left[\left(\frac{\mu}{Pr_k}\right)\nabla k\right] - \rho \varepsilon + \dot{W}^s \tag{3-4}$$

$$\frac{\partial(\rho\varepsilon)}{\partial t} + \nabla\cdot(\rho\boldsymbol{u}\varepsilon) = -\left(\frac{2}{3}c_{\varepsilon_1} - c_{\varepsilon_3}\right)\rho\varepsilon\nabla\cdot\sigma + \sigma:\nabla\boldsymbol{u} + \nabla\cdot\left[\left(\frac{\mu}{Pr_\varepsilon}\right)\nabla\varepsilon\right] + \frac{\varepsilon}{k}\left[c_{\varepsilon_1}\sigma:\nabla\boldsymbol{u} - c_{\varepsilon_2}\rho\varepsilon + c_s\dot{W}^s\right] \quad (3\text{-}5)$$

where,

$\dot{W}^s$:	turbulent eddies rate of work on spray dispersion
Pr:	Prandtl number, with constant model values for k and ε
c:	model constants

3.2 Original KIVA Sub-Models

The basic KIVA-4 program consists of sub-models that describe in-cylinder processes such as valve and piston movement, fuel injection, droplet interaction and evaporation, ignition, combustion and pollutant formation. Hence, the following section describes the original models relevant to this work which are subject to modification. Details or description of other original models is left to the original KIVA documentation.

3.2.1 Fuel library and multi-component fuel interaction

The basic fuel library in KIVA contains thirty-seven fuels that include, for example, paraffins, alcohols, aromatics, and fuel mixtures (gasoline and diesel). It also lists properties such as molecular weight, heating values and critical points as well as temperature-dependent properties (such as enthalpy and density). In addition to that, KIVA-4, includes the feature of multi-component fuels which enhances the representation of complex fuels and emerging fuel blends. However, with the increased attention towards alternative fuels, this library needs to be extended and developed as more data becomes available

3.2.2 Piston movement and snapping

The work due to piston movement plays an important role in the internal combustion engine. As the piston moves up from its bottom-most position, i.e bottom-dead-center (BDC), the volume of the combustion chamber decreases and the mixture temperature and pressure increases – consequently preparing the charge for spark- or auto-ignition. From a computational viewpoint, as the

volume of individual cells reduces due to piston movement, cells in the squish region will become very small and therefore the governing equations need be solved at very small time steps. For that reason, a process known as the snapper [28] is included to address this issue. During the compression stroke, as the piston moves from BDC towards the top-dead center (TDC), planes which volume reaches a preset threshold, usually half the original volume, deactivate. Conversely, as the piston motion reverses in the expansion stroke, those planes are re-activated. In other words, the activation/deactivation changes the total number of cells in the domain, and, as a result, total cylinder mass need be conserved during this process. This process is highlighted at this stage because an additional species density array is declared for the KIVA-CHEMKIN interface and it must pass through the snapper for proper mass conservation.

3.2.3 Ignition, combustion and pollutant formation

There are two main objectives of the chemistry solver; to predict the ignition (start of combustion) and combustion (evolution of species) as well as to estimate pollutant formation. The default chemistry solver in KIVA assumes a global single-step reaction, such as that in Equation (3-6) for tetra-decane oxidation, to predict the ignition and combustion of the mixture. This equation suggests full combustion where dissociation and intermediate species are ignored.

$$2\,C_{14}H_{30} + 43\,O_2 \rightarrow 28\,CO_2 + 30\,H_2O \tag{3-6}$$

Furthermore, the rate of the overall fuel oxidation is given by:

$$k_f = A^{\beta}\ exp\left(-\frac{E}{R\,T}\right)\ [C_{14}H_{30}]^m\ [O_2]^n \tag{3-7}$$

where,

k_f:	forward rate for overall reaction
A:	pre-exponential factor = 2.2×10^{11} (model parameter)
β:	temperature exponent = 0.00
E	effective activation energy = 30 kcal/mol (constant)
R:	universal gas constant
m:	fuel concentration exponent = 0.25 (varies by fuel)
n:	oxidizer concentration exponent = 1.50 (varies by fuel)

A value for the pre-exponential parameter, directly related to the heat release rate (HRR), is suggested for different fuels. However, this parameter, *A*, should, and often it must, be adjusted to prevent unrealistic heat release which will cause the code to fail or a small heat release which will not sustain combustion. According to the KIVA-3 manual [28], however, the use of mixing-controlled chemistry model reduces the need to adjust this parameter.

When solving for the chemistry source terms, i.e. species densities and heat release, a time savings technique is enforced where a temperature cut-off value is specified by the user such that cells below that value will skip the chemistry calculation. Adjustment of the pre-exponential parameter and the cut-off temperature value may be used to match experimental results for a given engine. Yet, this adjustment decreases credibility of the simple chemistry solver if such adjustments were arbitrary for different operating conditions.

Furthermore, to study and reduce engine-out emissions, the chemistry model needs to provide accurate species evolution information. Derived from the fact that the basic combustion model has limited capabilities, the emission prediction for CO and unburned hydrocarbon (HC) will, therefore, suffer from the same deficiencies. As a result, it is often the case that the user inserts additional global kinetic steps to represent NO_x formation and oxidation, commonly using the Zel'dovich model. In addition, KIVA uses an empirical model for soot, per Suroviki and Nagle/Strickland-Constable models, which does not depict the complex evolution of the process as understood today [11]. As such, the ignition and combustion model represents an active area for development efforts.

3.3 Past Improvements to KIVA

While the biggest portion of KIVA is developed by LANL, its open-source feature makes it an excellent educational tool where researchers build on the sub-models to enhance its predictive capabilities and bridge the gap between experimental observations and mathematical models. At the Engine Modeling Laboratory at the University of Illinois, KIVA-3VR2 [27] is the version which has

been used over the past decade. Over this period, researchers at the university have built upon and/or replaced existing models as they develop better understanding of the physical process from experimental studies, such as the insights gained from the DIATA optical engine[29]. For the present work, however, KIVA-4 is used instead and the reader is reminded of the lack of the enhanced features the following models offer to the overall model capability.

3.3.1 Ignition, combustion and pollutant formation

Autoignition of the fuel, using the Shell model, was first implemented by Shazi [30] in order to model compression ignition combustion and compare against experimental data obtained from the then-metal DIATA engine [29]. Shazi used tetra-decane ($C_{14}H_{30}$) as the diesel surrogate and was able to validate his model against the Thornton Rapid Compression Machine (RCM). When applied to engine simulations, the model matched experimental data with a pre-exponential factor of 1.4×10^4. The temperature cut-off value, which determines the start of combustion, was increased from 1,100 to 1,150 K. Furthermore, Shazi [30] implemented the Zel'dovich mechanism for modeling NO_x emission.

Wang [31] enhanced the Shell model by accounting for the mass balance through freezing the species rates at 950 K. Furthermore, Wang optimized the twenty-six kinetic parameters of the model to predict the auto-ignition on a range of temperatures, pressures, equivalence ratios and EGRs. Lastly, Wang improved the pollutant formation models by implementing the Hiroyasu model (soot formation) and Nagle and Strickland-Constable model (soot oxidation). Moreover, Stringer [32] built on the combustion model to take into account the oxygen depletion rate associated with oxygenated fuels. As a result, KIVA fuel library estimates the oxygen depletion rate for non-oxygenated fuels internally such that minimal interference is needed when users specify different fuels.

3.3.2 Fuel library

Stringer [32] expanded the KIVA fuel library to include five sources of biodiesel which are based on soybean, rapeseed, coconut, and palm oils and lard.

The new biodiesel library covers a wide range of physical properties and chemical structures which was used to study biodiesel sprays and combustion. Using a utility called BDProp, developed by Yuan [33], the fatty acid profile of each fuel was used to estimate properties such as density, viscosity, surface tension, latent heat of vaporization, vapor pressure and enthalpy.

3.3.3 Crevice flow model

There may exist inevitable leakage in the crevices between the piston rings and cylinder liner, which reduces the cylinder peak pressure due to the lower mass. This effect might be neglected in conventional metal engines, where the presence of a film of oil reduces such leakage. However, in optically-accessible engines such as the DIATA engine [29] neglecting the blow-by flow over-predicts the cylinder pressure by at least 10%. In response, Zhao [34] implemented a Namazian crevice model to account for the effects of the crevice on the cylinder mass and pressure. As a result, the enhanced feature makes comparison between experimental data and KIVA more plausible.

3.3.4 Multi-component fuel model

Another modification to KIVA-3 takes into account the evaporation of multi-component fuels which enhances representation of fuels physical properties. Both gasoline and diesel are mixtures of fuels which could be represented better by more than one surrogate. Similarly, with Stringer's [32] addition of biodiesel species in the fuel library, the multi-component fuel evaporation addition makes modeling of diesel-biodiesel blends more accurate. The model was developed by Chin [35] and it assumes that each fuel could have up-to four components. The combustion rate constants and other properties of the multi-component fuel are determined by weighing the contributions of each constituent with their mole fractions. Further, Zeng [36] and Wang [31] developed the model by enhancing the evaporation of the multi-component fuel droplets and films. They achieved computational time savings by implementing continuous thermodynamics which no longer requires solving the transport equations for each component. It is

worth mentioning that the LANL version of KIVA-4 has a built-in multi-component fuel model, [37], which is based on [36].

3.3.5 Spray impingement model

A common result of direct fuel injection is spray splashing or deposit on cylinder wall. Trujillo [38], added a model to account for spray impingement to study the associated increase in cold-start emissions due to the fuel-rich films on piston bowl and cylinder walls. Trujillo's model takes into account surface roughness which more accurately models droplet splash and deposit. The resulting change to droplet diameter and velocity is calculated using a probability density function (PDF) optimized using empirical constants.

3.3.6 Spray breakup model

One of the most important processes in direct-injection simulations is the spray atomization and breakup which influences the ignition and combustion of the mixture. By default, KIVA uses the Taylor-Analogy Breakup (TAB) model, which models the droplet interaction as a spring-mass system. Such model was observed to over-predict the relative velocity between the liquid droplet and the surrounding gas due to lower drag coefficients. Consequently, the droplet diameter size would be smaller, vaporizes faster and therefore the cylinder pressure and heat release are over-predicted.

Yuan [33] improved the spray model by implementing the Kelvin-Helmholtz Rayleigh-Taylor (KH-RT) breakup model. In the KH-RT model, two instabilities are competing against one another for liquid fuel breakup. The Kelvin-Helmholtz instability develops due to the velocity difference between the droplet and surrounding gas whereas the Rayleigh-Taylor instability occurs due to the deceleration or deformation of the droplet. The Rayleigh-Taylor model is used with the Kelvin-Helmholtz model to calculate the secondary breakup of droplets. The model was recently modified by Stringer [32] to model biodiesel fuels.

CHAPTER 4: THE CHEMKIN SOFTWARE PACKAGE

One of the most common approaches to coupling the CFD solution with detailed chemistry is through integration with a chemistry solver, such as CHEMKIN or CANTERA through an application programming interface (API) where a user-defined program is written to interact between the two software packages. The purpose of the interface program is to obtain the temperature, pressure and species information from each cell as solved in KIVA. After that, this information is passed to CHEMKIN which consequently solves for the change in species densities and heat release, which obey a set of governing equations. For this research, the API was developed to interact between CHEMKIN and KIVA. Thus, it is at this point that CHEMKIN, the de-facto standard for chemistry applications, is introduced.

4.1 General overview of CHEMKIN

The Fortran-based Chemical Kinetics package, hence the name CHEMKIN, was originally developed at Sandia National Laboratory [25] for the analysis of gas-phase chemical and plasma kinetics. It contains a powerful set of utilities that enables solving for the chemistry source terms in reactive flow applications. It is the most commonly used software package for such an application.

The first and most important input a chemistry solvers needs is a reaction mechanism file and the associated thermodynamic properties database. The reaction mechanism file begins by declaring the elements and species involved in the reactions. After that, it contains symbolic representation of each reaction step, and the Arrhenius rate coefficients, given in the right-hand side of Equation (4-1). For a given reaction, i, these coefficients are the pre-exponential factor, temperature exponent and the activation energy.

$$k_{f_i} = A_i \, T^{\beta_i} \, exp\left[-\frac{E_i}{R_c \, T}\right] \tag{4-1}$$

where,

k_{f_i}: forward reaction rate

A_i: pre-exponential factor

T: temperature
β_i: temperature exponent
E_i: activation energy
R_c: universal gas constant

In addition to the reaction data, a database of thermodynamic properties, in format similar to the NASA standard, must be available either separately or embedded into the mechanism file, which declares atomic weights, polynomial-fit parameters for standard-state enthalpy, entropy and specific heat relations, and the applicable temperature range. The input files, i.e. the reaction mechanism and thermodynamic database, must undergo a pre-processing step to generate a binary linking file which is used by the program to solve the problem.

Because KIVA is written in Fortran, the CHEMKIN interface program was chosen to be written in Fortran. A system of ordinary differential equations (ODE), outlined in the next chapter, is defined and solved using the latest version of VODE, the variable-coefficient ODE solver [18].

CHAPTER 5: MODEL DEVELOPMENT

The current work focuses on the development of a new combustion sub-model which directly couples the KIVA CFD solution with detailed chemistry as solved by CHEMKIN. Thus, it is important that development is incremental to ensure proper numerical implementation and stability within KIVA. As highlighted in Section 3.3, the current version of the code used in the Engine Modeling Lab at the University of Illinois is KIVA-3VR2 which has been extensively improved by past graduates, [30]-[36] and [38]. Such development enhances physical and chemistry sub-models, yet at the same time increases the complexity of the code and associated debugging process.

Therefore, and for simplicity, an *original* version of KIVA is proposed as the development ground for the detailed chemistry sub-model. Hence, the latest release of the software, KIVA-4 [26], is used instead of the in-house version of KIVA-3VR2. In doing so, the model as a whole will not provide the best physical representation, especially due to lack of detailed spray dynamics and crevice flow sub-models, since the associated computational cost is deemed too expensive for development purposes.

5.1 Interaction of the New Code with KIVA

The model is developed entirely for KIVA-4 structure which is written in Fortran 95, offers enhanced memory access and allocation, and readily enables code parallelization. The new combustion model, called `detchem.f`, overrides the call to the original KIVA chemistry solver `chem.f` (referenced throughout the text as the "default chemistry solver") based on a flag in the simulation input file, `itape5`. Once the detailed chemistry model is called, it updates only two variables; (1) species densities and (2) heat release which are the chemistry source terms shown in Equations (2-3) and (2-4). Based on the change in density, the vapor mass is updated. Furthermore, the cell enthalpy and internal energy are updated by adding the amount of energy released from chemical reactions. Please note that although the change of temperature is calculated

within `detchem.f` using Equation (2-2), this value is not passed directly to KIVA. Instead, `tsolve.f`, which calculates the change in temperature throughout the CFD simulation cycle, would solve the new temperature using the updated species densities and mass fractions. This formulation is consistent with the original chemistry model (`chem.f`) and the general structure of KIVA.

In addition to the following KIVA-4 default input files:

1. simulation input file, `itape5`,
2. computational grid file, `kiva4grid`, and
3. species enthalpy data file, `datahk`.

a forth input file is needed when the detailed chemistry subroutine is called. The file is a binary linking file, named `cklink`, and is produced using the CHEMKIN pre-processor. While the grid file remains unchanged, specific instructions must be followed in preparing the remaining input files. The following sub-sections describe the required steps.

5.1.1 Reaction Kinetics Files

Based on the literature review and validation of its application to engine simulations, the ERC revised n-heptane mechanism [14] is used for all modeled cases in this work. The mechanism consists of 52 elementary reactions and 29 species which do not include NO_x formation/oxidation reactions – although a common approach is to integrate it with the Zel'dovich mechanism. The associated thermodynamic database was not modified. However, a single modification was performed on the mechanism by including nitrogen and nitrogen oxide in the species list (without participation in any reaction). This modification was shown to have no implication on the kinetic solution using single-zone constant-pressure adiabatic combustion simulations. The reason for this modification is merely to maintain the memory locations for these species which are already allocated by KIVA.

5.1.2 CHEMKIN Linking File

Before the CHEMKIN library could be used, the reaction mechanism (`mech.dat`) and thermodynamic database (`therm.dat`) files must be pre-processed to generate a binary linking file (`cklink`), through a CHEMKIN-supplied utility. Once the linking file is written, the interface program in KIVA requires it as an additional input file. While this pre-processor could be considered as a black-box, problems could arise between KIVA and CHEMKIN if the order of species is not consistent since KIVA relies on the array indices (rather than chemical formula) to update variables. As a check-point, therefore, KIVA input reader, `rinput.f`, was modified with a logic that checks for the consistency of species listings (or order) in the linking file and KIVA. The user must re-arrange the listing of species in the mechanism file (`mech.dat`) to be consistent with KIVA `itape5`. Please note that the user must re-generate the linking file (`cklink`) after any changes to either `mech.dat` or `therm.dat`.

5.1.3 CHEMKIN-to-KIVA Pre-Processor

The first actual step towards integrating CHEMKIN with KIVA is to use a shared set of species data and thermodynamic properties. It is assumed that the thermodynamic database provided with the reaction mechanism is most appropriate for a given application and hence should over-ride default values in KIVA. This is enabled in KIVA-4 which recognizes existence of such need and accordingly requires an additional input file (`datahk`) for species enthalpy data. Thus, relevant to this work, KIVA-4 requires mechanism-specific modifications to two input files; (1) the simulation specification file, `itape5`, and (2) the enthalpy data file, `datahk`.

In `itape5`, KIVA requires a table containing species information, such as species formulas, molecular weights and heats of formation, as well as a composition table that contains a character string followed by the initial mass fractions of the mixture. For illustration, the two sections in `itape5` requiring

modifications are shown in Appendix A which shows entries of the default 12 species using tetra-decane as fuel with air as the initial mixture.

The enthalpy data file, `datahk`, on the other hand, contains enthalpy data for all gaseous species (except the fuel whose enthalpy is obtained from the KIVA fuel library) and other reference values. An excerpt from `datahk` is shown in Appendix B. Fifty-one enthalpy points, which correspond to the enthalpies from 0 to 5,000 K in 100 K intervals, (in kcal/mol units) are inserted. The enthalpy block is followed by the critical temperature and pressure, and an acentric value.

To automate the process of generating these sections in the `itape5` and `datahk` files, a pre-processor program, called CHEMKIN-to-KIVA (abbreviated to `CK2KIVA`) was developed. `CK2KIVA`, easily creates the composition tables which list the species formulas, molecular weights, heat-of-formation and mass fractions for the all species participating in the detailed chemistry using CHEMKIN libraries. A sample output is shown in Appendix B (were default KIVA species are omitted only to save paper). Please note that the converter, by design, does not compute the mass fractions since the pre-processor is only supposed to be executed once for each mechanism file.

The pre-processor, `CK2KIVA`, also creates the new `datahk` file which contains all the information described above. The enthalpy data is extracted from CHEMKIN libraries, while the critical values require manual retrieval. The critical temperature and pressure values are obtained from the NIST Chemistry WebBook. Lastly, the acentric value is entered. Since no clear definition of this value is provided in KIVA-4 manual, and because there was no direct impact on either of the critical values or acentric value, a value of zero could be assigned to species unique to the reaction mechanism.

5.2 Basic Combustion Model

The governing equations, (2-1) to (2-4), represent the constant-volume combustion which could be directly implemented for HCCI applications.

However, the heat addition in diesel combustion occurs at a constant-pressure, and accordingly Equation (2-2) is modified to include the enthalpy and specific heat at constant-pressure:

$$\frac{dT}{dt} = -\frac{1}{\rho\ \bar{c_p}} \sum_{k=1}^{K} \dot{\omega}_k\ W_k\ h_k \qquad (5\text{-}1)$$

where,

$\bar{c_p}$: cell averaged specific heat at constant pressure

h_k: specific enthalpy for species k

As a result, the modeling of HCCI and DI requires a different temperature rate equation according to (2-2) and (5-1), respectively. To automate such selection, one could compute the rate of pressure change and use it as a criterion for the temperature rate of change. Another general approach which is applicable to both constant-volume and constant-pressure combustion is a constant-volume approximation provided that the integration time step is small, which is in the order of 1 μs which effectively assures the volume of the computational is constant over a number of time steps.

Therefore, the governing equations based on constant-volume combustion, (2-1) to (2-4), were used as the default system of equations since this approach is shown to be appropriate for both HCCI and DI applications. Moreover, to facilitate the comparison of the effects of Equations (2-2) and (5-1) on the solution, a conditional statement was employed allowing the user to force constant-pressure combustion, if needed.

5.3 Scaling of Species Composition

For convenience, it was of interest to limit the number of species in KIVA to the default 12 species, while the total species involved in CHEMKIN is that specified in the mechanism file. This limitation aims to reduce the memory requirement for spray calculations. The CHEMKIN solution from the previous chemistry calculation is saved in a new species density array. This array, however, must pass through the piston snapping subroutine which will adjust the number of cells as the piston approaches its upper most position (TDC) as

described in Section 3.2.2. In other words, a reduced number of species in the fluid cycle could be specified (in the simulation input, `itape5`) to be less than that in the mechanism input file (`mech.dat`). This approach is meant for convenience only, and on short-term basis, to reduce memory utilization for DI applications which could not be executed otherwise in the current workstation. In response, the following approach to weight or scale the contribution of different species is proposed if the number of species in `itape5` is less than the number of species participating in chemical reactions. First, the species are classified into three categories, illustrated in Figure 6-1; (1) reference species which are the species of the stoichiometric reaction, (2) primary species which are the remaining KIVA species by default, and (3) auxiliary species which are all the remaining species in the chemical mechanism file.

The composition scaling was performed on the species mass fractions, for simplicity, as described below. After the first chemistry calculation, not necessarily the first call to CHEMKIN, the new array of species densities is saved. Based on the chemistry solution, the KIVA species density array is modified as follows: First, the CHEMKIN density array is converted into mass fractions, using Equation (2-3). After that, the mass fractions of reference species remain unchanged in both KIVA and CHEMKIN since these species exhibit the biggest contribution of mass fractions. Second, the mass fractions of all auxiliary species are set to zero in the KIVA array. As a result, mass conservation is applied to the primary species according to the following equation:

$$Y_{Pri}^{CFD} = Y_{Pri}^{Chem} \times \frac{\sum Y_{Pri}^{Chem}}{1 - \sum Y_{Ref}^{Chem}} \tag{5-2}$$

where,

Y: species mass fractions

subscripts,

Ref: Index for reference species (which range from 1 to `nspl`+4) where `nspl` is the number of liquid species (i.e. fuel components specified in `itape5`, which equals 1 in all present simulations)

Pri: Index for primary species (which range from `nspl`+5 to `nsp`) where `nsp` is the total number of species specified in `itape5` (e.g. 12)

superscripts,

CFD:	KIVA solution
Chem:	CHEMKIN solution

which scales up the mass fractions of the *primary* species due to reduction of mass contribution from *auxiliary* species.

The terms used to classify the species, i.e. reference, primary and auxiliary, are used with reference to their status in KIVA and are in no way implied to disregard their importance in the reaction pathways. It is therefore stressed that this methodology works acceptably for the specific application of the ERC n-heptane mechanism and no generalization is made otherwise.

5.4 Characteristic Time Cut-Off Criteria

In the default chemistry model, a common approach to speed-up the computation is to apply a temperature cut-off limit below which the chemistry calculation is skipped. The temperature criterion is justified for chemistry models when the reaction rates are temperature independent, however, that is not the case when elementary reactions are implemented. As a result, using the same approach for detailed chemistry calculation is likely to affect ignition timing and heat release. Consequently, a characteristic time approach is implemented in the new combustion model.

The molar production rate, $\dot{\omega}_k$, is expressed in terms of the creation rate and destruction time as:

$$\dot{\omega}_k \equiv \dot{C}_k - \dot{D}_k = \dot{C}_k - \frac{[X_k]}{\tau_k} \tag{5-3}$$

where,

$\dot{C}_k$:	species creation rate
$\dot{D}_k$:	species destruction rate
τ_k:	destruction characteristic time

If the destruction time is long, compared to the hydrodynamic time step, then the molar production rate is equal to the creation rate, i.e. there is no change to species concentration. Accordingly, there is no justification to spend computer

time in said cells. Thus, the current model calculates the characteristic destruction times for all species as obtained from the CHEMKIN library based on initial species composition and cell temperature. If the minimum characteristic time (for all species) in a given cell is larger than the hydrodynamic time step, then chemistry calculation is skipped. Otherwise, the detailed chemistry solver, `detchem.f`, is in effect with a fixed integration time step (1 μs).

CHAPTER 6: RESULTS AND DISCUSSION

The developed coupled CFD-chemistry model is not validated until it has been demonstrated that it predicts experimental data fairly well. However, due to the limited sub-models implemented in KIVA-4, the model is likely to fall short in its predictive capability at this stage. As a result, the purpose of this section is to show that the model is capable of predicting the general trends for both HCCI and DI combustion without any model adjustments. Furthermore, this section discusses the implications of the simplifications made during the development on the simulated results.

6.1 Model Predictions under HCCI Conditions

This discussion is based on pre-mixed HCCI simulations of diesel fuel on the LION engine, although no such operation has been attempted. The chemistry was solved using the coupled `detchem.f` code and compared against `chem.f`. The diesel oxidation is simulated using the skeletal mechanism of n-heptane, developed by [14], which effectively consists of 29 species and 52 species. As described in Section 5.1.3, two additional species (N and NO) was inserted in the reaction mechanism file to save their corresponding memory locations in KIVA. These two species did not participate in any reaction since the NO_x mechanism was not implemented. The total number of species, therefore, became 31 within both of CHEMKIN and KIVA cycles. The heat flux into the chamber was based on a constant wall temperature specified in the input `itape5`. Four computational domains, shown in Figure 6-2, were used in the simulations. The initial temperature and pressure were fixed for all simulated results at 370 K and 1.1 bar, respectively.

The development of `detchem.f` was closely related to predictions from `chem.f`. In other words, throughout the basic development of the coupled CFD-chemistry model, detailed computer output from the default chemistry subroutine, `chem.f`, was used to debug the new code, `detchem.f`. Furthermore, the study of fumigated HCCI cases reduces the complexity of early injection

modeling and saves time. As a result, this section will clarify a number of uncertainties about the basic implementation procedures for the coupled CFD-chemistry model.

6.1.1 Effect of Different Physical/Chemical Properties

Briefly suggested in Section 5.1.3, since fuel surrogates are used to represent the chemical kinetics model, a different already-validated surrogate is used to represent the physical properties. Further, the model was built with the option to override the fuel enthalpy data in the KIVA fuel library with the updated values used in the development of the reaction mechanism (i.e. based on `therm.dat`). This study is conducted merely to clarify some of the concerns which emerge when multi-component fuels (or fuel blends) are used. The following results illustrate this process.

Figure 6-3 compares the combustion of n-heptane (chemically and physically) using the detailed chemistry and default KIVA solvers. Essentially, the solid lines represent the ideal implementation of the fuel physical and chemical properties. The enthalpy data for n-heptane is closely related in KIVA fuel library and in the thermodynamic database file, which is shown by the overlap of dashed and solid lines of a given model. Therefore, the differences between `chem.f` and `detchem.f` are solely based on the kinetic model.

In most cases, however, it is desired to model the diesel fuel using a heavier surrogate, namely tetra-decane, which will accordingly have different physical properties than n-hetpane, the kinetic surrogate. Since the base model is based on conservation of mass fractions, the user would safely input tetra-decane as the fuel in KIVA, and CHEMKIN will use the first species in the mechanism file as the fuel surrogate. Figure 6-4 illustrates a successful representation of the two-stage combustion, ignition timing, and total heat release in this approach. It must be highlighted that due to the nature of HCCI combustion, i.e. pre-mixed vaporized fuel, the physical characteristics of the fuel do not seem to affect the simulated results.

6.1.2 Effect of Species Composition Scaling

Due to memory allocation limitation, the number of KIVA species was reduced to 12, which is the default number of species in KIVA. This feature, i.e. limited number of species in KIVA regardless of number of participating species in the reaction file, is likely to go along with established post-processing models which are programmed for assigned locations on species variable arrays.

Based on the composition scaling proposal, Section 5.3, HCCI simulations were carried out as shown in Figure 6-5. Both pressure and total heat release charts show the two-stage combustion. Furthermore, the charts indicate that reducing the number of species advances the onset of combustion by a fraction of a degree, and slightly reduce peak values. This trend is explained by the selection criteria for the reference and primary species which was arbitrarily based on the importance of KIVA default species. As a result, it is very likely that neglecting key species in the reaction mechanism will impact the combustion characteristics. The deviation was within an acceptable range for HCCI combustion, but that might not be the case for DI simulations.

6.1.3 Representation of General Trends

In addition to comparing the solution of the coupled CFD-chemistry code developed in this study, comparison was made with the optimized Shell ignition model implemented in KIVA-3VR2 alongside the default KIVA chemistry solver. Figures 6-6 and 6-7 show a comparison of the pressure and temperature histories for tetra-decane HCCI combustion with equivalence ratios, ϕ, of 0.4 and 0.2, respectively. The two-stage combustion is captured by the detailed chemistry solver for both equivalence ratios as the step rise of pressure, temperature and heat release around 350°. The peak pressure and temperature agrees well for all three models indicating correct implementation of the new code. However, the heat release rate calculation in KIVA-4 seems lower than its counterpart estimated by KIVA-3VR2 – which may require further investigation. As the equivalence ratio decreases, the ignition predicted by the new code,

detchem.f, compared to the traditional combustion models is delayed by 10 degrees. This trend was observed in constant-volume kinetic combustion which suggests increase in ignition time with decreased equivalence ratio. This is in fact a control strategy to delay ignition and commonly achieved through high amounts of EGR. This feature, however, is not re-produced in the Shell or default ignition/combustion models unless the pre-exponential factor was modified (and no such adjustment was made in this study).

6.1.4 Justification for model numerical optimization

In order to give an indication of the computational cost or time associated with detailed chemistry calculations using detchem.f, a profiling program was used to measure the simulation run time. Table 6-3 summarizes the computation time for pre-mixed HCCI combustion using all four grids shown in Figure 6-2. The detailed chemistry calculation is 50 times longer than the execution time of the default chemistry model using the 2D meshes. That variance increases drastically as the number of cells increases in the domain. For instance, the detailed chemistry computation time using the high-resolution 3D grid is 7.5 hours which compares to a convenient 1.5 minutes in chem.f. In other words, the current model, without numerical optimization techniques, does not provide a convenient predictive tool due to the prolonged run times. More importantly, the computation time will further increase in direct-injection simulations due the reduced hydrodynamic time step required to resolve spray dynamics. Therefore, one of the most important future improvements is to include some of the optimization techniques described in Section 2.4.

6.2 Model Predictions under DI Conditions

The following discussion is based on direct injection simulations of diesel fuel on the LION engine. The chemistry calculations were solved using the coupled detchem.f code. The diesel oxidation is simulated using the skeletal mechanism of n-heptane used in HCCI simulations, however, the number of species in the KIVA calculations was reduced to 12, per the procedure described

in Section 5.3. The sub-models used in the simulations were the TAB spray breakup model and the RNG k-ε turbulence model. The heat flux into the chamber was based on the constant wall temperature value specified. Only the low-resolution grids, Figure 6-2, were used for direct-injection simulations, unless noted otherwise.

6.2.1 Representation of General Trends

Before the model could be validated against experimental data, it must show first that it is capable of capturing the general trends of direct-injection combustion. For this study, a single injection event with 20 mg/cycle of diesel is injected within 15 degrees of the variable injection timing. A fixed EGR rate of 40% was used to dilute the mixture. As shown in Figure 6-8, two sets of results for different start-of-injection (SOI) timings are present; the solid line is the prediction of the detailed chemistry solver, `detchem.f`, while the dotted lines correspond to the default KIVA chemistry solver, `chem.f`. The fuel specified in KIVA is tetra-decane, while the n-heptane mechanism is used in CHEMKIN.

Since no kinetic parameters were adjusted (in neither of the subroutines), Figure 6-8 shows the deficiency of `chem.f` which fails to simulate the onset of combustion, or ignition, due to the lack of the Shell model. On the other hand, the integrated detailed chemistry model successfully predicts the relation between SOI and ignition. In other words, earlier SOI provides ample time for fuel to mix which therefore advance ignition, and increase peak pressure and temperature. The early injection case, SOI = 330 CAD, replicate the results from premixed HCCI where the homogeneous mixture is rapidly ignited resulting in the highest peak temperature. Furthermore, the two-stage ignition is observed in the trends for SOI = 330 and 340 CAD. Lastly, the rate of temperature or pressure rise is high for all simulated cases as would be expected in the perfectly-stirred reactor (PSR) formulation.

6.2.2 Challenges of Model Validation

The challenges of model validation against experimental data begin with predicting the motoring or pre-firing pressure trace. In engine experiments, it is very difficult to measure the temperature at inlet valve closure (IVC). In response, an iterative approach is commonly employed in KIVA to estimate the temperature at IVC as the initial mixture temperature of the closed-cycle simulation. First, the initial mixture composition is estimated and in such case an air mixture with no EGR was used. After that, the experimental value of pressure at the inlet valve closure is entered as the initial mixture pressure. Next, an initial temperature value is estimated based on manifold temperature and the KIVA simulation is started. The initial temperature is iterated until the produced pre-firing pressure curve is in agreement with experimental data.

Two single-injection cases were conducted using the metal LION engine, [29], details of which are shown in Table 6-5. For Case 1, the manifold pressure was 1.176 bar, while the manifold temperature was 308 K. In attempt to match the pre-firing curve of this case, a number of combinations of initial temperature and pressure produced a good match with experimental data, as shown in Figure 6-9a. As can be seen, at least two independent combinations of initial pressure and temperature produce an acceptable match to the experimental pressure trace. One possible source of error is the lack of a crevice model, which from experience in KIVA-3VR2 simulations exhibit higher pressure trace. As a result, the initial pressure values in Figure 6-9a were smaller than the manifold pressure to compensate for the lack of the crevice model.

The dependence of the solution on the selected initial temperature is not negligible, as can be seen in Figure 6-9b, where the initial mixture temperatures at TDC differ by 80 K in the simulated curves. As a result, a deviation in ignition timing of 5 CAD is observed. Furthermore, the heat release rate shows a big variation in comparison with the experimental trend which indicates a number of things. First, the reduced number of species in KIVA might have contributed to low heat release since it depends on the species mass fractions.

Second, the early ignition could be linked to the rapid fuel vaporization resulting from the TAB model. In addition, the heat release has a sharp and narrow profile which is consistent with the kinetics-controlled heat release curves, e.g. Figure 2-3. This conclusion is also supported by the nearly-vertical rate of change in temperature and pressure inherent in the kinetics-controlled formulation of the current model. Needless to say, the difficulty of validating single-injection cases will be magnified in low-temperature combustion where multiple injection events take place.

6.2.3 Effects of Using Cut-Off Temperature

One approach to speed-up conventional chemistry calculations in KIVA is to implement a temperature cut-off criterion, below which the chemistry calculation for the subject cell is skipped. Implementation of such criterion in the detailed chemistry subroutine must not be enforced since there is no clear criteria based on temperature that determines if significant change in molar production rates has taken place. To illustrate, Figure 6-10 shows the pressure, heat release and temperature profiles for a direct-injection case. Four cut-off temperatures were used which are 300, 700, 750 and 800 K. Please note that all previous simulations used a cut-off temperature of 300 K which is lower than the initial intake temperature. Consequently, it is viewed as the correct solution since all cells in the domain are subjected to the reaction kinetics. Use of higher cut-off temperatures, i.e. T_{cut} = 750 and 800 K, yields higher heat release rate and longer ignition delay. A marginal cut-off temperature was used, 700 K, which results indicate lower temperature and higher heat release. The ignition, on the other hand, seem to agree with the baseline case, i.e. T_{cut} = 300 K. As a result, the use of a cut-off temperature is found to alter the prediction of the model. Therefore, the model was enhanced to internally force the cut-off temperature to a value equivalent to the inlet temperature and the alternative cut-off criterion was based on the chemical characteristic time described in Section 5.4.

6.2.4 Justification of constant-volume approximation

Lastly, as described in the Section 5.2, the model was formulated to solve the detailed chemistry at each computational cell as a constant-volume, adiabatic combustion per the governing equations, (2-1) to (2-4). This assumption is based on common approach to increase model applicability to both HCCI and DI combustion. In order to justify this assumption, Figure 6-11 shows a comparison of the pressure and heat release rate as computed by both constant-pressure and constant-volume models. The figure clearly correlates both solutions as they predict the ignition and combustion fairly well. It is worth noting that this simulation was based on a low-resolution 3D mesh, depicted in Figure 6-2b, which an initial simulation pressure of 1.125 bar and temperature of 370 K. The heat release rate curve clearly indicates a calculation problem in the 3D species since the peak of the heat release rate chart in the 2D simulation is 3.5 times higher than that produced by the 3D simulations.

6.3 Tables

	Equivalence Ratio, ϕ		
Species	0.2	0.4	0.6
C_7H_{16}	0.01301	0.02568	0.03803
O_2	0.22846	0.22552	0.22267
N_2	0.75854	0.74880	0.73930

Table 6-1: Initial species mass fractions for HCCI simulations using n-heptane.

	Equivalence Ratio, ϕ		
Species	0.2	0.4	0.6
$C_{14}H_{30}$	0.01317	0.02600	0.03850
O_2	0.22842	0.22545	0.22256
N_2	0.75841	0.74855	0.73894

Table 6-2: Initial species mass fractions for HCCI simulations using tetra-decane.

HCCI	`chem.f`	`detchem.f`
2D Coarse Mesh	10 sec	9 min
2D Fine Mesh	40 sec	38 min
3D Coarse Mesh	1 min	42 min
3D Fine Mesh	1.5 min	7.5 hr

Table 6-3: Comparison of HCCI simulation times using four grids.

Engine Feature	Specification
Engine Type	Ford Lion
Number of Cylinders	6
Cycle	4-stroke diesel
Induction System	Variable geometry turbocharger
Number of Intake Valves	2
Number of Exhaust Valves	2
Combustion Chamber	Direct injection
Bore	81 mm
Stroke	88 mm
Displaced Volume	453.46 cm3
Clearance Volume	27.82 cm3
Compression Ratio	17.3 : 1
Connecting Rod Length	160 mm
Fuel Injection System	Common rail (up to 1650-bar pressure)
Fuel Injector Type	Piezoelectric with 6 nozzles
EGR	Water-cooled EGR pumps

Table 6-4: LION Engine Specifications [29].

	Case 1	**Case 2**
Fuel	Ultra low sulfur diesel	
Engine speed (rpm)	1,500	2000
Load (bmep)	5	7 bar
EGR Ratio (%)	0	0
Intake manifold press (bar)	1.176	1.342
Intake air temp (°C)	35	45
Start of Injection (ATDC)	0.7	-0.88
Injection Duration (ms)	0.59	0.57
Mass of fuel injected (mg/cycle)	15.43	19.52

Table 6-5: Experimental conditions for DI LION engine.

6.4 Figures

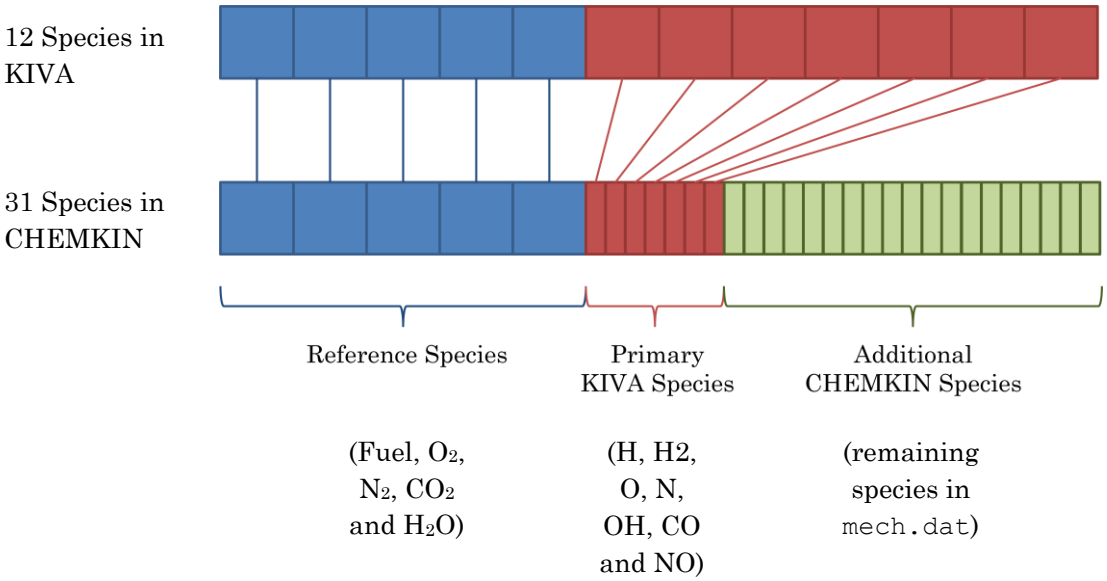

Figure 6-1: Schematic of the mass scaling process.
This approach is implemented if the number of species in KIVA is desired to be less than that in CHEMKIN.

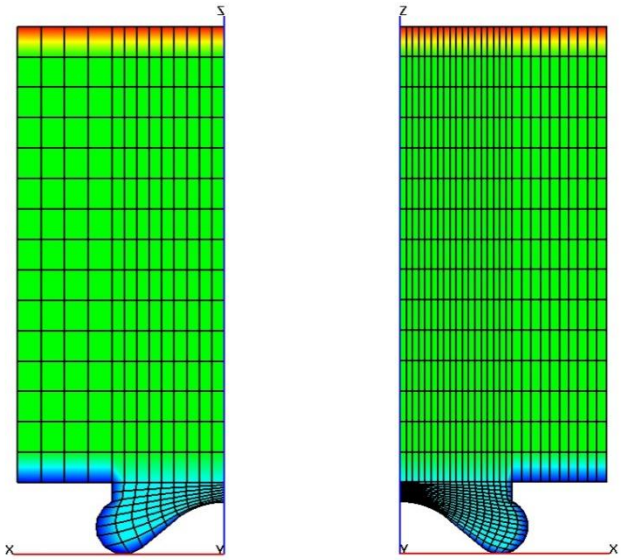

267 Cells
584 Nodes

708 Cells
1,504 Nodes

(a)

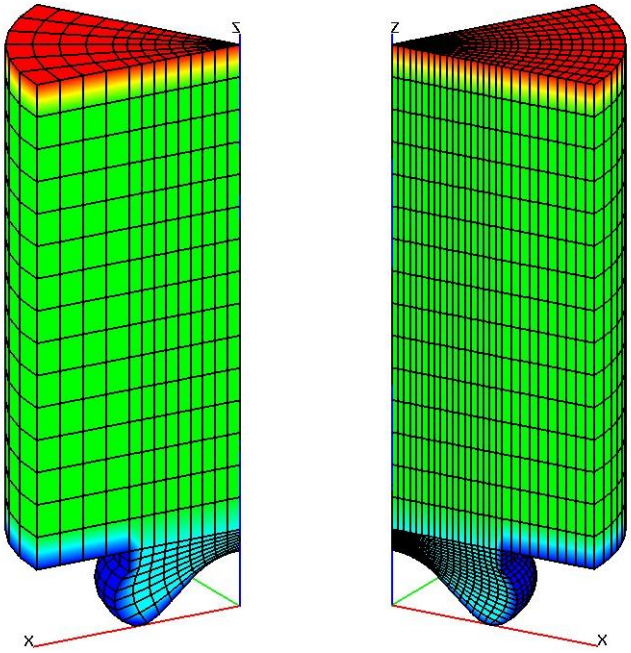

1,602 Cells
1,984 Nodes

8,496 Cells
9,600 Nodes

(b)

Figure 6-2: The computational domains for the LION engine used in this study. Figure (a) coarse and fine 2D meshes, and (b) equivalent 3D 60°-sector grids. Grids are colored by the cell boundary conditions.

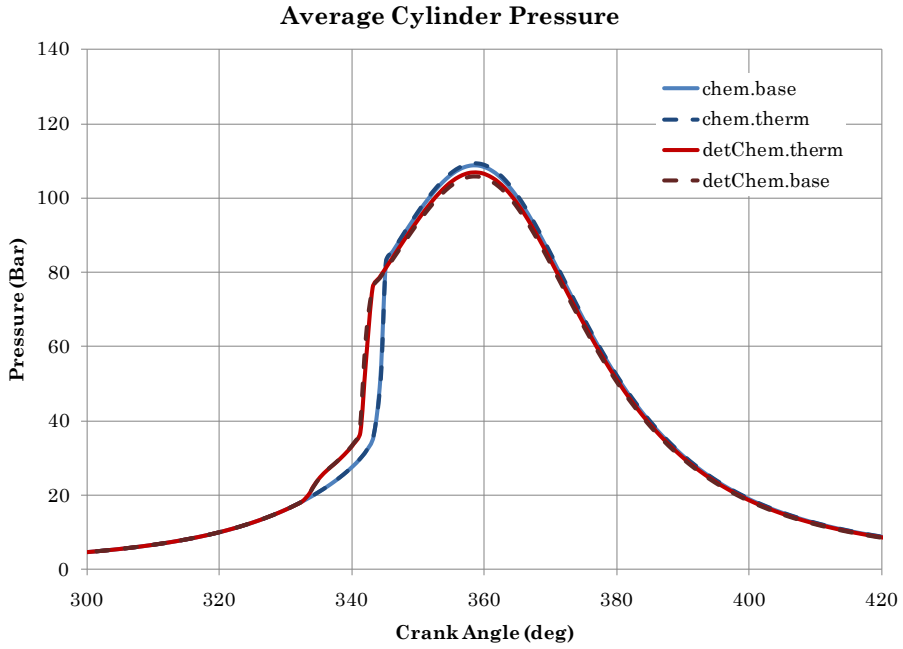

(a)

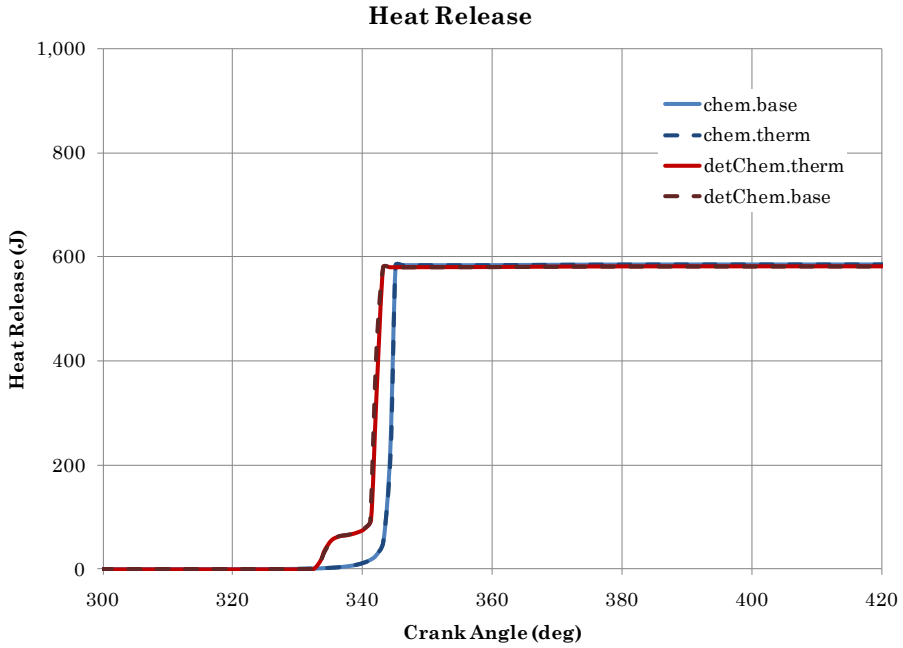

(b)

Figure 6-3: Comparison of effect of enthalpy data source on (a) pressure, and (b) total heat release using physical/chemical properties of n-heptane. Blue line corresponds to `chem.f` solutions while red lines represent `detchem.f` simulations. Solid lines conform to the default source of enthalpy data, whereas the dashed lines show the alternative enthalpy data set.

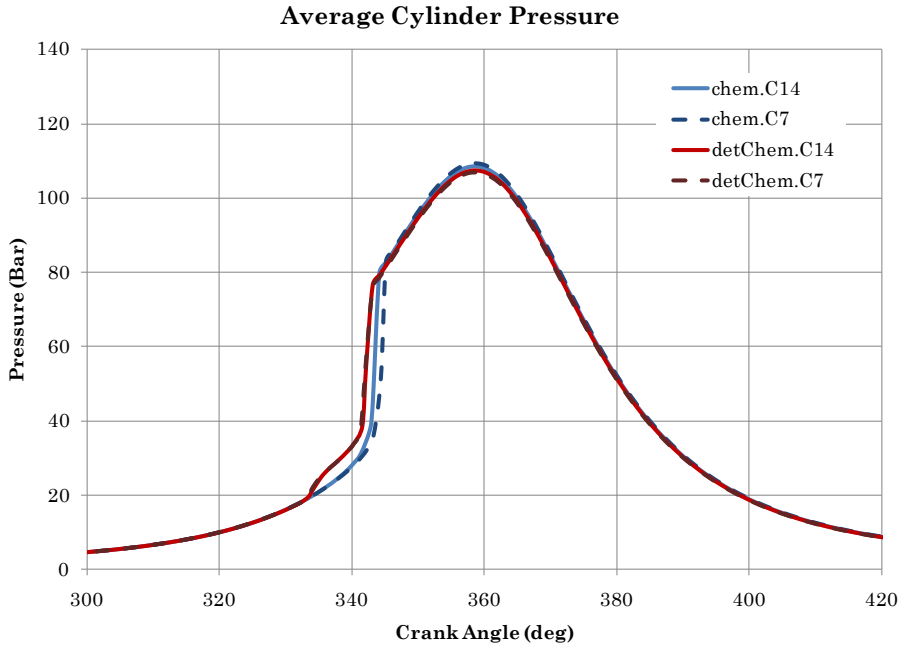

(a)

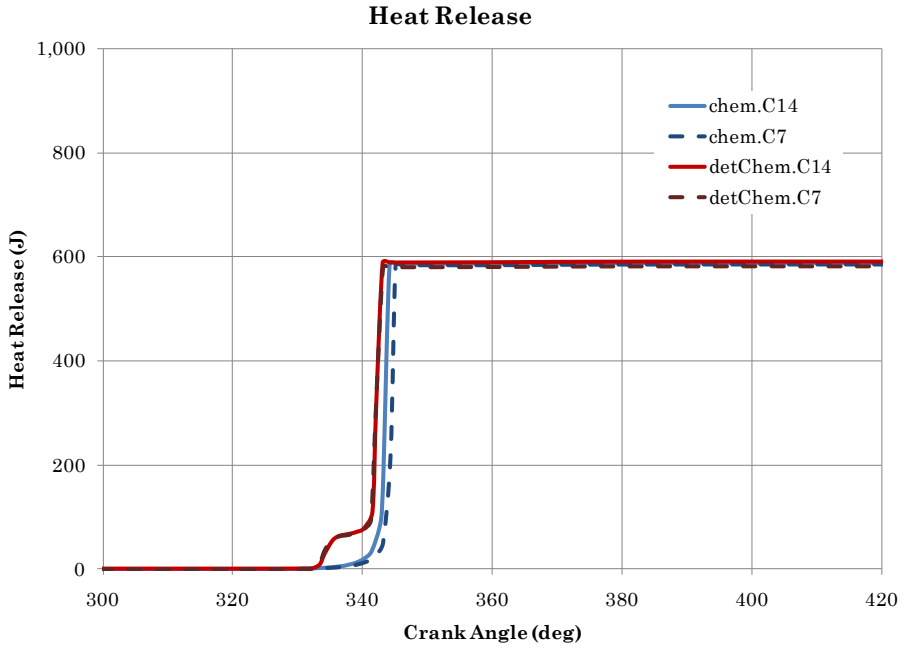

(b)

Figure 6-4: Comparison of effect of different physical-chemical properties of the fuel on (a) pressure, and (b) total heat release.
Blue line corresponds to `chem.f` solutions while red lines are for `detchem.f`. Dashed lines conform to the physical and chemical properties of n-heptane, whereas solid simulations use n-heptane as the surrogate for tetra-decane.

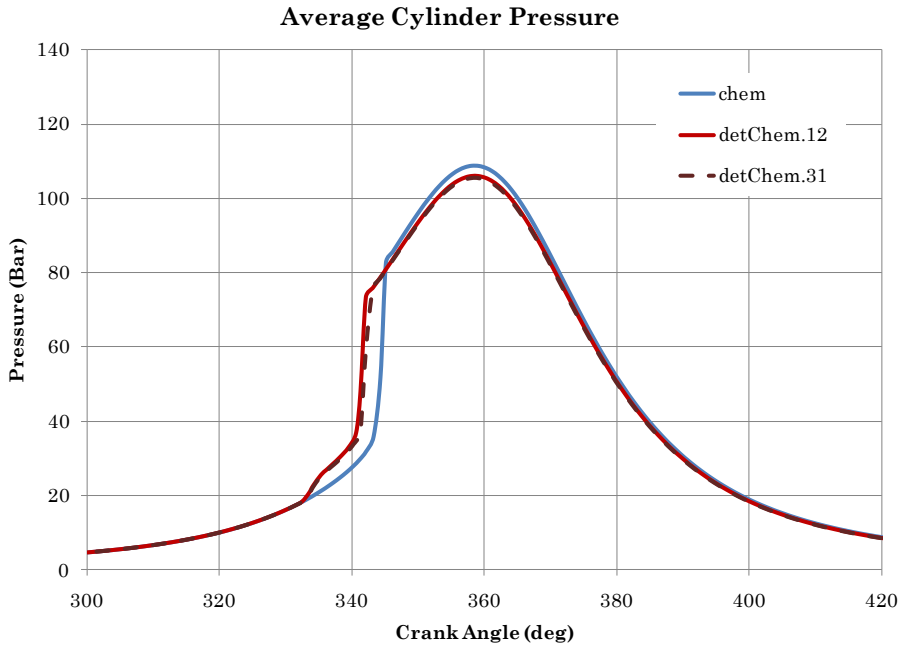

(a)

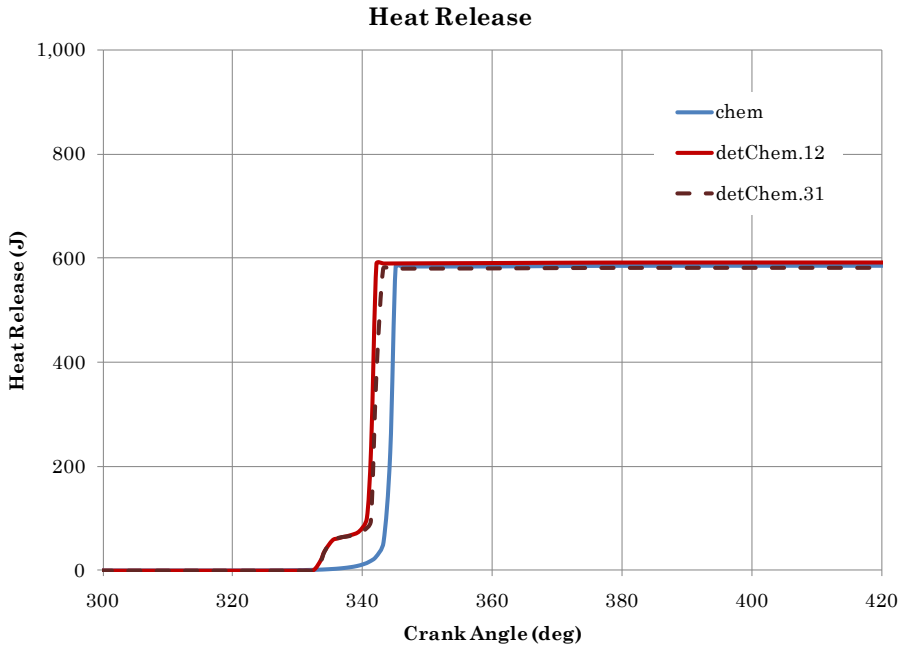

(b)

Figure 6-5: Comparison of effect of reducing the number of species in the CFD cycle on (a) pressure, and (b) total heat release.
Blue line corresponds to `chem.f` solution, red dashed line represents the full CHEMKIN species solution, while the red solid line (staggered) shows the proposed reduced number of species in KIVA.

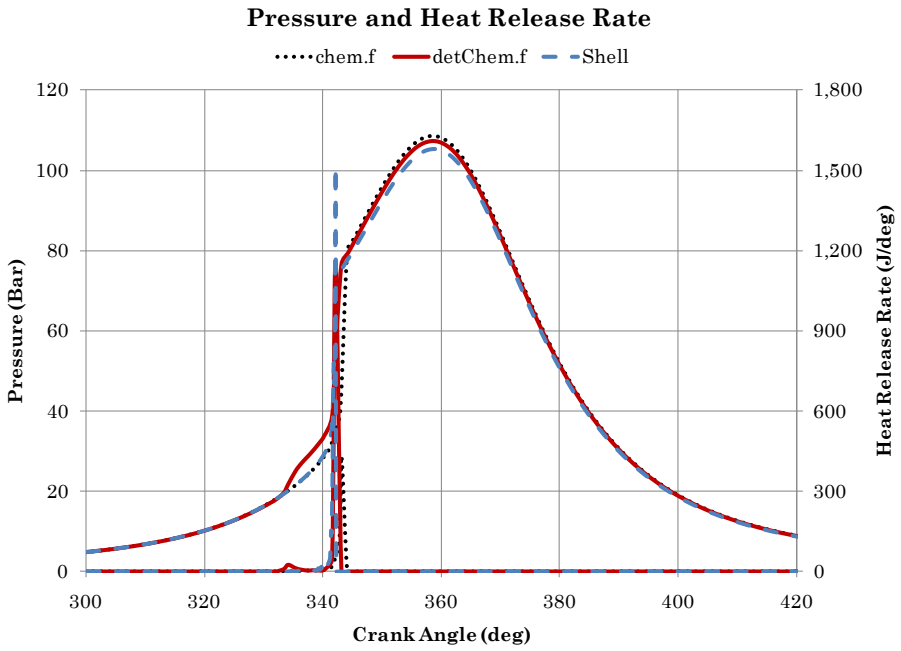

(a)

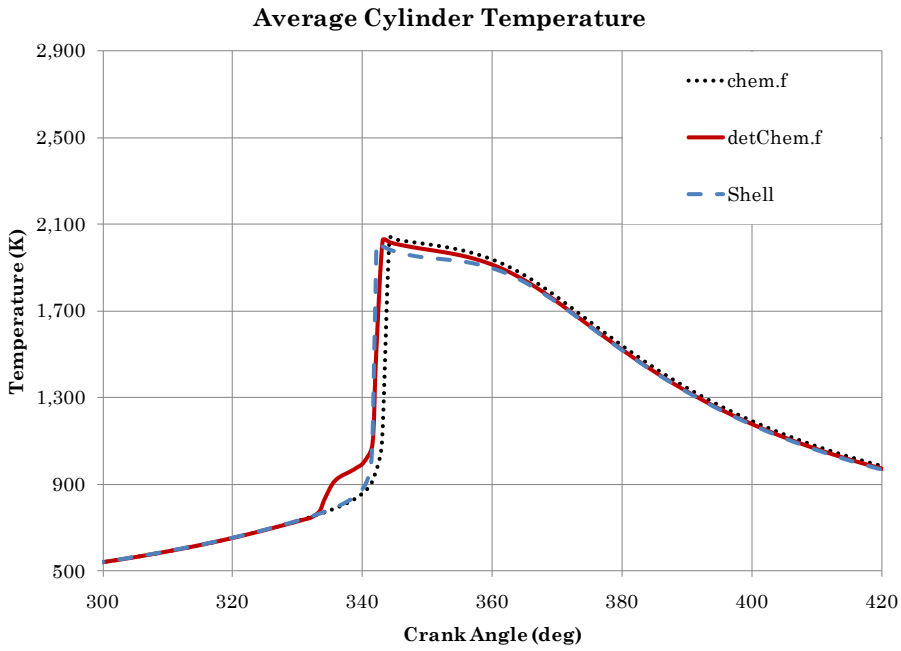

(b)

Figure 6-6: Comparison of calculated cylinder (a) pressure and (b) temperature ($\phi = 0.4$). Dotted line is the default chemistry model in KIVA4, solid line is the new detailed chemistry solver in KIVA4, and the optimized Shell model implemented in KIVA-3VR2 is the dashed line.

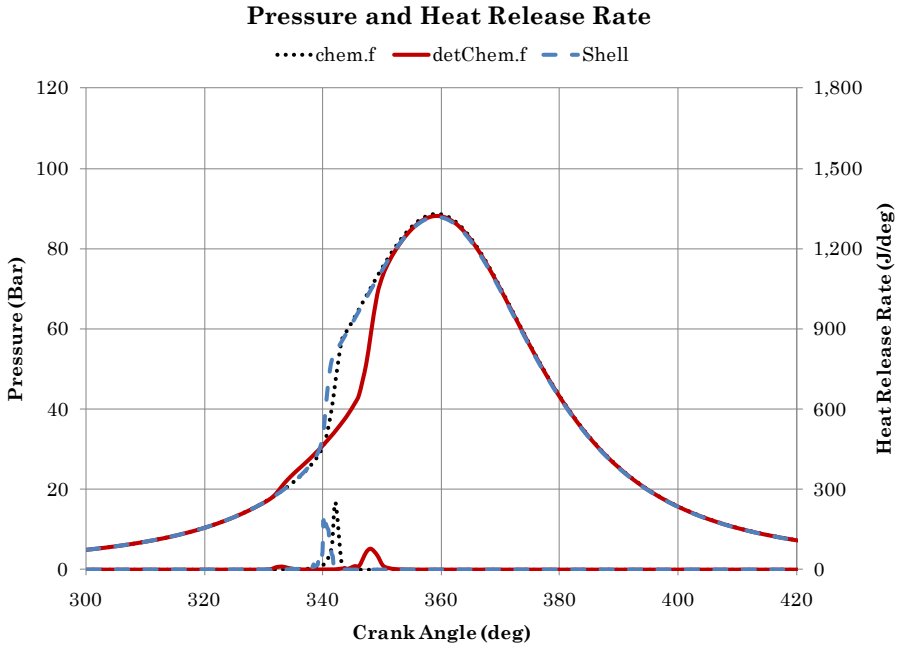

(a)

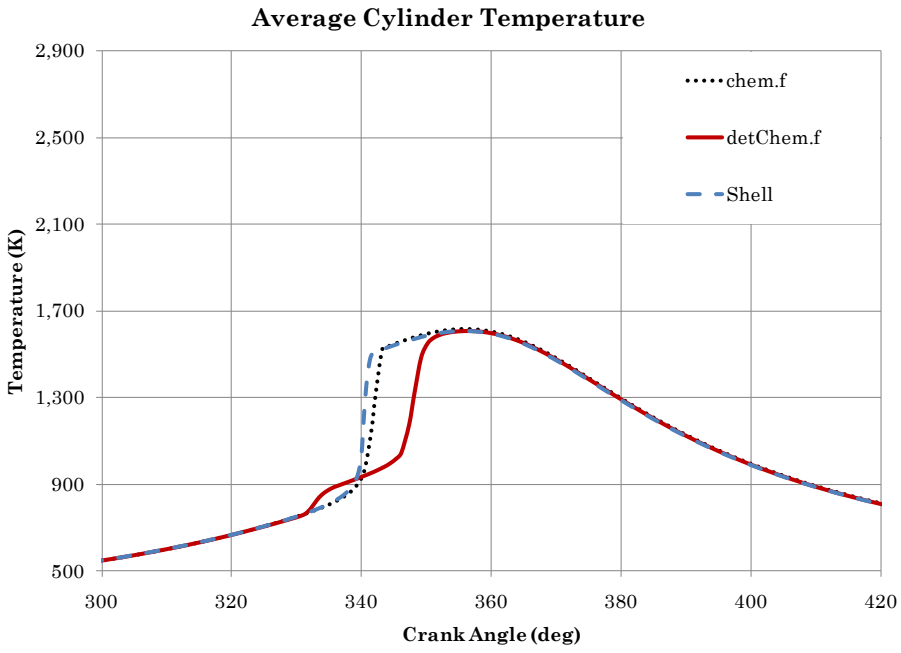

(b)

Figure 6-7: Comparison of calculated cylinder (a) pressure and (b) temperature ($\phi = 0.2$). Dotted line is the default chemistry model in KIVA4, solid line is the new detailed chemistry solver in KIVA4, and the optimized Shell model implemented in KIVA-3VR2 is the dashed line.

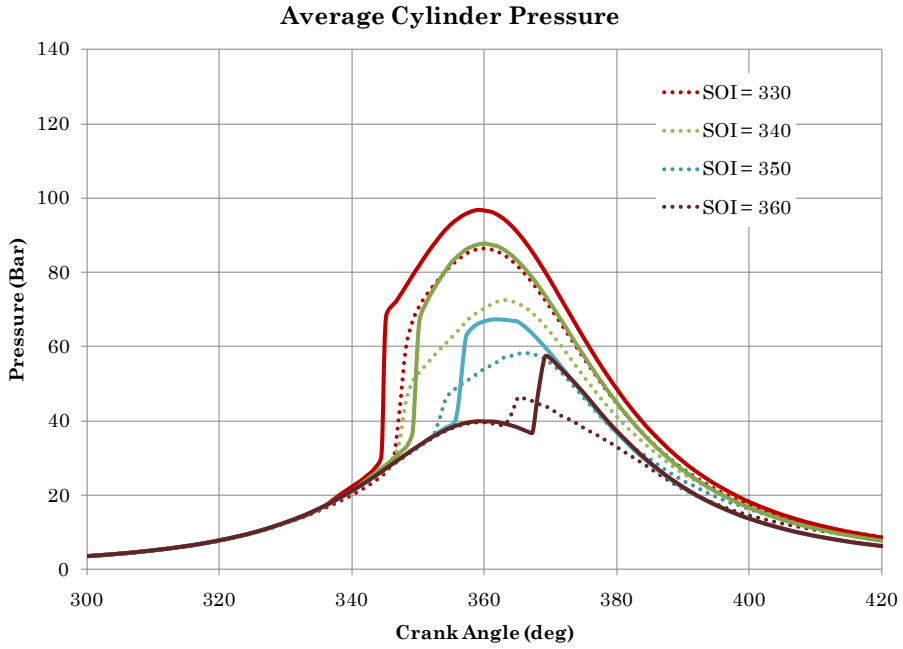

(a)

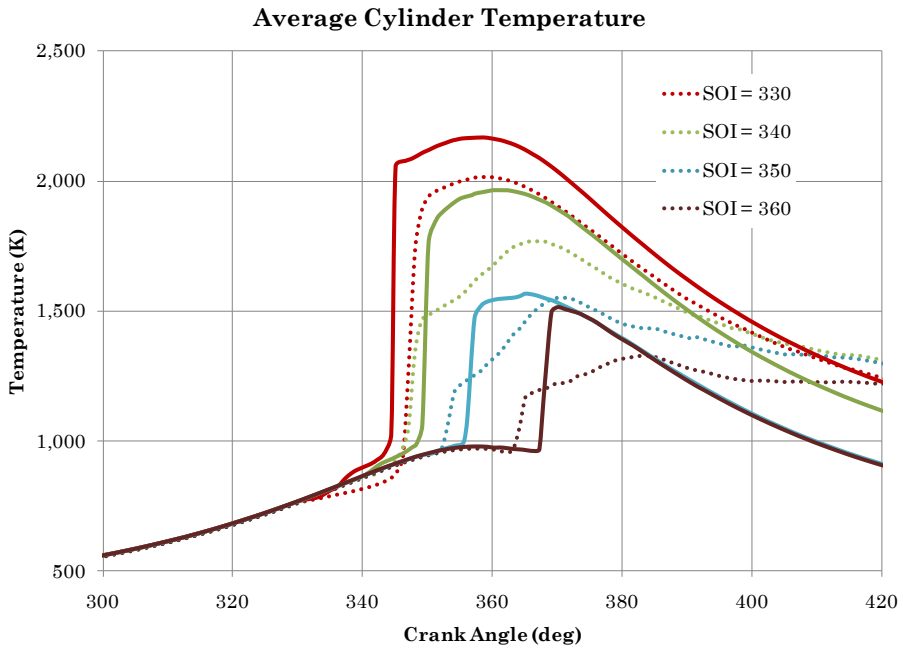

(b)

Figure 6-8: Predictions of general trends for DI combustion showing (a) pressure and (b) temperature histories.
ID = 15 CAD, 40% EGR. Solid lines represents `detchem.f`, while dotted lines are `chem.f` predictions of with no adjustment to kinetic reactions.

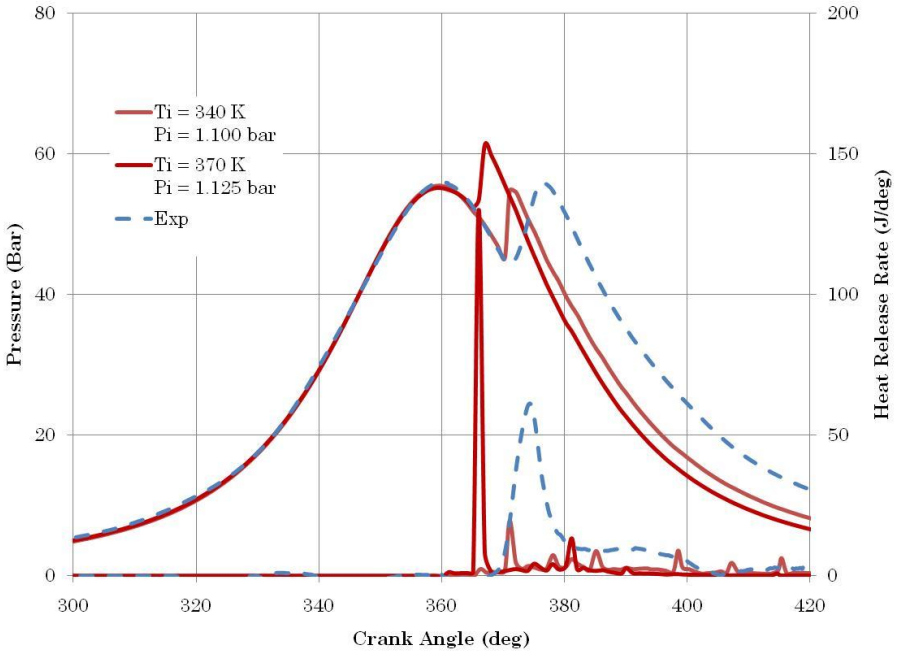

(a)

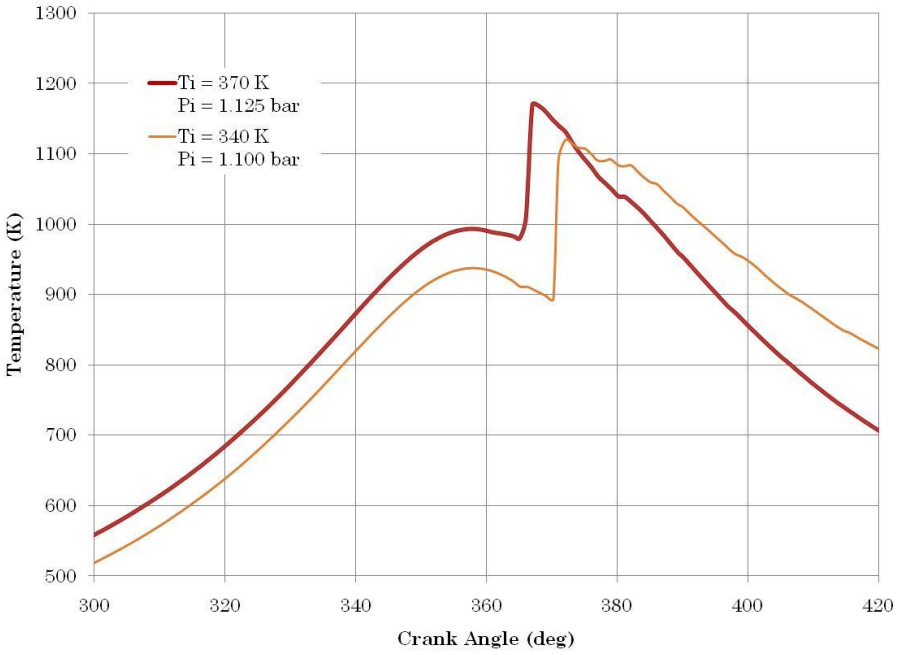

(b)

Figure 6-9: Sensitivity of initial inlet conditions on (a) pressure and (b) temperature. Experimental data (dashed line) corresponds to Case 1 of Table 6-5, while solid lines are simulated results.

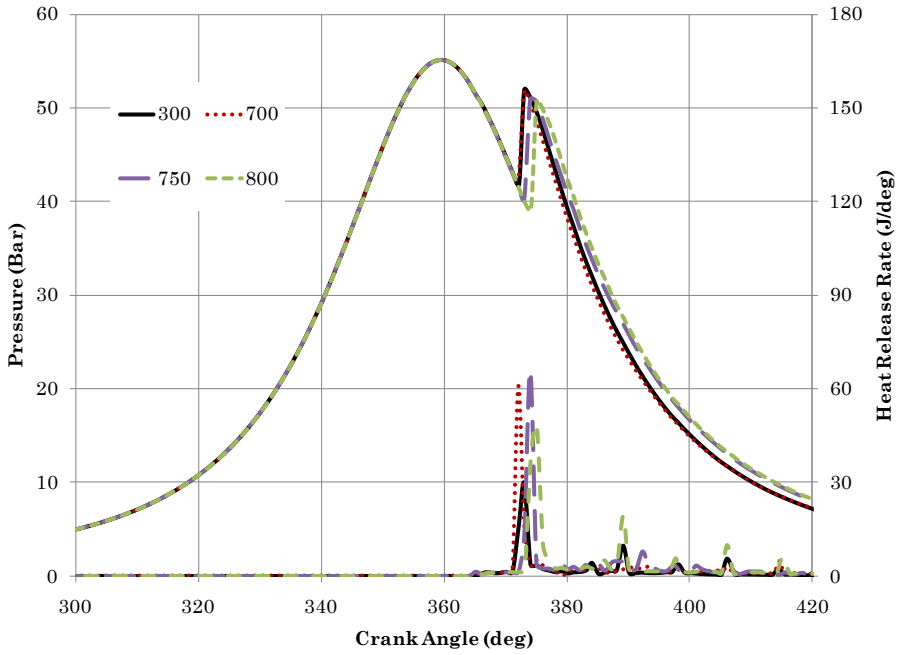

(a)

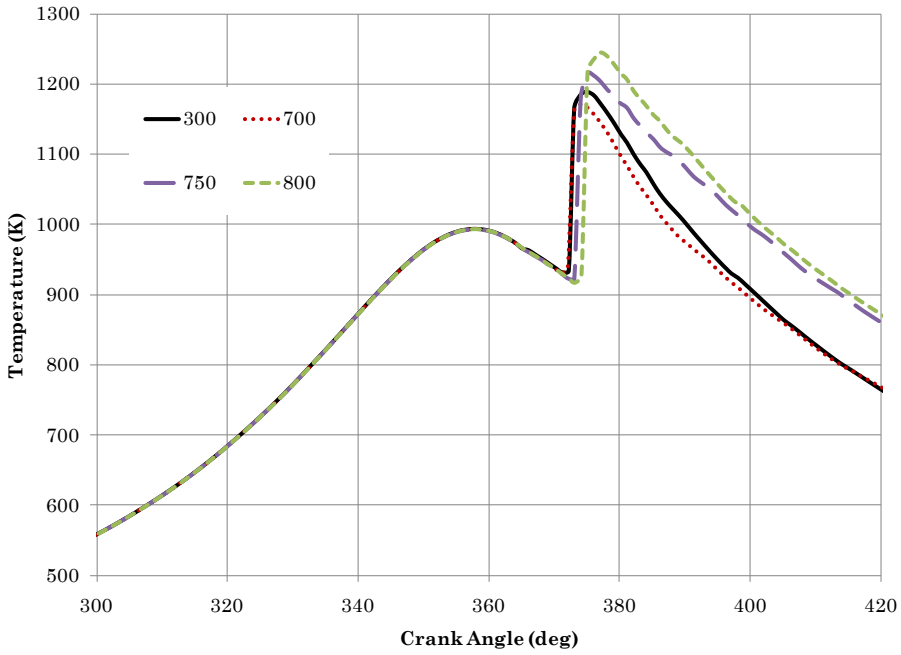

(b)

Figure 6-10: Effects of cut-off temperature on (a) pressure and heat release, and (b) temperature.
All lines are simulated results.

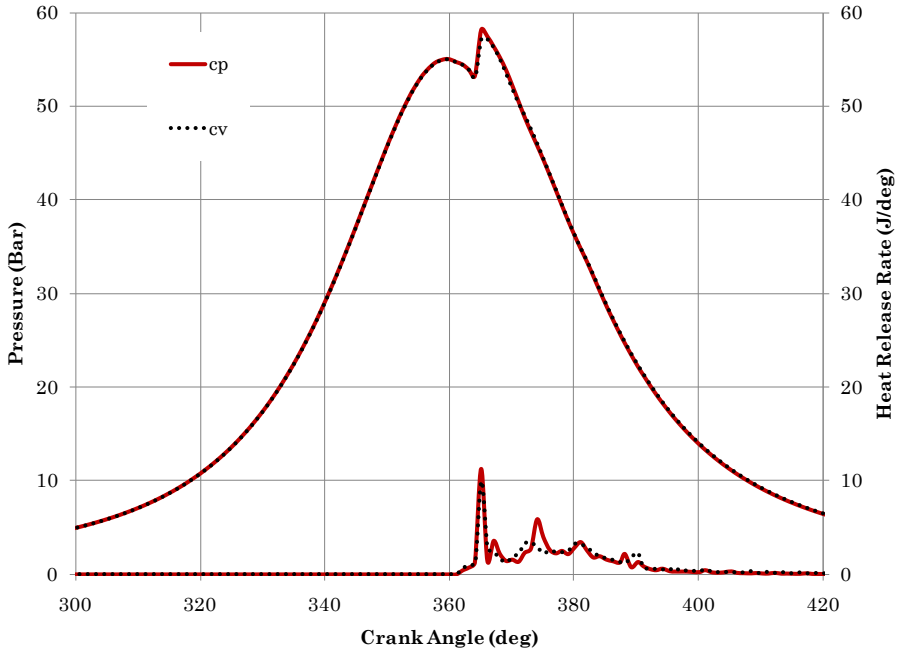

Figure 6-11: Comparison of pressure and heat release computed using both constant-volume and constant-pressure combustion models.
Solid lines show the solution using constant-pressure formulation, whereas the constant-volume approximation is given by the dotted line.

CHAPTER 7: CONCLUSIONS

7.1 General Conclusions

This study successfully demonstrated a first model that couples the computational fluid dynamics solution from KIVA with detailed chemistry solved by CHEMKIN. Although the model was not validated against experimental data, it was shown to clarify some implementation uncertainties and provide the general trends. The following conclusions are drawn:

1. Through balance of mass fractions, the use of different surrogates (i.e. different fuel species for physical and chemical processes) is established. Accordingly, the use of a single, well-established, engine-friendly kinetic model (i.e. primary reference fuel) is promoted.
2. The discussed results were based on a single reaction mechanism, the ERC n-heptane mechanism, which kinetic parameters remained un-altered in all studied cases.
3. Despite the high computational cost associated, the detailed chemistry solution is robust in predicting – rather than matching – experimental trends, which will greatly enhance the model credibility once validated.
4. From ignition and combustion phasing point of view, simulation of pre-mixed HCCI combustion could be successfully reproduced in low-resolution, two-dimensional domain. Simulation of practical HCCI-like combustion (through early injection) has also been successfully achieved.
5. Deviation from experimental results in DI simulations could be explained by assumptions made in the development of this first-hands model, and will be highlighted as areas of future improvement.

7.2 Future Work

As stated in the Model Development Section, this work aims to be a foundation for future development to the integrated chemistry-CFD model for engine and biodiesel research at the University of Illinois. Thus, it is paramount

that necessary improvement is highlighted to complement this project and validate the model. Recommendations for future work, therefore, are prioritized as follows:

1. The model was developed in isolation of crucial sub-models, such as Kelvin-Helmholtz Rayleigh-Taylor spray and blow-by models. It is crucial that such sub-models be implemented in KIVA-4, or, inversely, the detailed chemistry subroutine be migrated to KIVA-3VR2 for enhanced overall simulations.
2. As present, the model only addresses fuel oxidation, ignition and combustion. To truly capitalize on the computational burden of detailed chemistry, kinetic reactions for NO_x and a model for soot must be included for emission studies.
3. The most important feature currently lacking is the inclusion of sub-grid turbulence models. Of the reviewed models, implementation of the turbulent-mixing effects in a perfectly-stirred reactor might be appropriate for the structure of the current model.
4. The short-term approach of limiting the number of species in KIVA and CHEMKIN does indeed affect the spatial species evolution in the cylinder. Accordingly, full species evolution must be included to enhance the spatial contribution to emissions formation and oxidation.
5. The code profiling output should be used to further optimize the code call tree with respect to CHEMKIN subroutines. Such optimization could be extended to parallelize the CHEMKIN interface using OpenMP.
6. Further optimization, through multi-grid optimization techniques where the chemistry is solved in a low-resolution domain based on high-resolution CFD solution is critical to speed-up the model and enabling parametric studies.
7. Ignition results show strong sensitivity to estimated inlet temperature. A first-principles, full-cycle model, taking into account engine layout, would provide better pre-firing temperature profile and enhance model predictions.

REFERENCES

1. BUCKLAND, J. H.; COOK, J. A. Automotive Emissions Control. **American Control Conference**, p. 3290-5, 2005.

2. JOHNSON, T. V. **Diesel Emission Control in Review.** SAE International. Warrendale, PA. 2008. (Paper 2008-01-0069).

3. HEYWOOD, J. B. **Internal Combustion Engine Fundamentals**. New York: McGraw-Hill, 1988.

4. BAUMGARTEN, C. **Mixture Formation in Internal Combustion Engines**. Berlin: Springer, 2006.

5. KONG, S.-C.; REITZ, R. D. Numerical Study of Premixed HCCI Engine Combustion and its Sensitivity to Computational Mesh and Model Uncertainties. **Combustion Theory and Modelling**, v. 7, p. 417-433, May 2003.

6. ACEVES, S. M. et al. **A Multi-Zone Model for Prediction of HCCl Combustion and Emissions**. SAE International. Warrendale, PA. 2000. (Paper 2000-01-0327).

7. ACEVES, S. M. et al. **A Decoupled Model of Detailed Fluid Mechanics Followed by Detailed Chemical Kinetics for Prediction of Iso-Octane HCCI Combustion**. SAE International. Warrendale, PA. 2001. (Paper 2001-01-3612).

8. KONG, S.-C.; REITZ, R. D. Use of Detailed Chemical Kinetics to Study HCCI Engine Combustion With Consideration of Turbulent Mixing Effects. **Journal of Engineering for Gas Turbines and Power**, v. 124, p. 702-707, July 2002.

9. LIANG, L.; PUDUPPAKKAM, K.; MEEKS, E. **Towards Using Realistic Chemical Kinetics in Multidimensional CFD**. 19th International Multidimensional Engine Modeling User's Group Meeting. Detroit, MI: Engine Research Center. 2009.

10. HONG, S.; WOOLDRIDGE, M. S.; ASSANIS, D. N. Modeling of Chemical and Mixing Effects on Methane Autoignition under Direct-Injection, Stratified Charge Conditions. **Energy Production**, v. 29, p. 711-718, 2002.

11. HONG, S. et al. Modeling of Diesel Combustion, Soot and NO Emission Based on a Modified Eddy Dissipation Concept. **Combustion Science and Technology**,

v. 180, p. 1421-1448, 2008.

12. GOLOVITCHEV, V. I.; NORDIN, N. **Detailed Chemistry Spray Combustion Model for the KIVA Code**. 11th International Multidimensional Engine Modeling User's Group Meeting at the SAE Congress. Detriot, MI: Engine Research Center. 2001.

13. MAGNUSSEN, B. F. **The Eddy Dissipation Concept:** A Bridge between Science and Technology. ECCOMAS Thematic Conference on Computational Combustion. Lisbon: ECCOMAS. 2005.

14. PATEL, A. **Development, Validation and Application of a Reduced n-Heptane Reaction Mechanism to Diesel Engine Combustion Optimization**. University of Wisconsin. Madison. 2004.

15. BRAKORA, J. L. **Development and Validation of a Reduced Reaction Mechanism for Biodiesel-Fueled Engine Simulations.** M.Sc Thesis: University of Wisconsin. Madison. 2007.

16. BABAJIMOPOULOS, A. et al. A Fully Coupled Computational Fluid Dynamics and Multi-Zone Model with Detailed Chemical Kinetics for the Simulation of Premixed Charge Compression Ignition Engines. **International Journal of Engine Research**, v. 6, p. 497-512, 2005.

17. SHI, Y.; HESSEL, R. P.; REITZ, R. D. An Adaptive Multi-Grid Chemistry (AMC) Model for Efficient Simulation of HCCI and DI Engine Combustion. **Combustion Theory and Moldeing**, p. 1-22, 2008.

18. BROWN, P. N.; BYRNE, G. D.; HINDMARSH, A. C. VODE, A Variable-Coefficient ODE Solver. **SIAM Journal on Scientific and Statistical Computing**, v. 10, n. 5, p. 1038-1051, September 1989.

19. AMSDEN, A. A.; O'ROURKE, P. J.; BUTLER, T. D. **KIVA-II: A Computer Program for Chemically Reactive Flows with Sprays.** Los Alamos. 1989.

20. LIANG, L. et al. Development of a Semi-Implicit Solver for Detailed Chemistry in Internal Combustion Engines. **Journal of Engineering for Gas Turbine and Power**, v. 129, p. 271-278, January 2007.

21. LI, Y. et al. **Parallel Computing of KIVA-4 Using Adaptive Mesh Refinement.** SAE International. Warrendale, PA. 2009. (Paper 2009-01-0723).

22. ALI, A. et al. **Improvement in Computational Efficiency for HCCI Engine Modeling by Using Reduced Mechanisms and Parallel Computing**. 13th

International Multidimensional EngineModeling User's Group Meeting. Detroit, MI: Engine Research Center. 2003.

23. SHI, Y. et al. **Efficient Multidimensional Simulation of HCCI and DI Engine Combustion with Detailed Chemistry**. SAE International. Warrendale, PA. 2009. (Paper 2009-01-0701).

24. KONG, S.-C.; HAN, Z.; REITZ, R. D. **The Development and Application of a Diesel Ignition and Combustion Model for Multidimensional Engine Simulation**. SAE International. Warrendale, PA. 1995. (Paper 950278).

25. KEE, R. J. et al. **CHEMKIN-III: A Fortran Chemical Kinetics Package for the Analysis of Gas-Phase Chemical and Plasma Kinetics**. Sandia National Laboratories. Livermore. 1996. (SAND96-8216).

26. TORRES, D. J.; TRUJILLO, M. F. KIVA-4: An Unstructured ALE Code for Compressible Gas Flow with Sprays. **Journal of Computational Physics (vol 219)**, p. 943–975, 2006.

27. AMSDEN, A. A. **KIVA-3V, Release 2, Improvements to KIVA-3V**. Los Alamos. 1999.

28. AMSDEN, A. A. **KIVA-3: A KIVA Program with Block-Structured Mesh for Complex Geometries**. Los Alamos National Laboratory. Los Alamos. 1993. (LA-12503-MS).

29. FOONG, T. M. **Setup of Common-Rail Small-Bore High-Speed Direct-Injection Diesel Engines for Biodiesel Combustion Studies**. M.Sc Thesis: University of Illinois. Urbana. 2009.

30. SHAZI, R. **Modeling the Autoignition, Combustion, and Pollutant Formation in a High-Speed Direct Injection Diesel Engine**. University of Illinois. Urbana-Champaign. 2002.

31. WANG, R. C.-P. **Modeling of a High Speed Direct Injection Diesel Engine Operating in HCCI Mode**. M.Sc Thesis: University of Illinois. Urbana. 2006.

32. STRINGER, V. L. **Modeling of Biodiesel Spray and Combustion of Biodiesel Fuels and Biodiesel Fuel Blends in a Direct Injection Diesel Engine**. M.Sc Thesis: University of Illinois. Urbana. 2007.

33. YUAN, W. **Computational Modeling of NOx Emissions from Biodiesel Combustion Based on Accurate Fuel Properties**. PhD Disseritation:

University of Illinois. Urbana. 2005.

34. ZHAO, J. **Modeling the Autoignition, Blow-By, and Pollutant Formation in a Small Bore High Speed Direct Injection Optically Accessible Diesel Engine**. University of Illinois. Urbana-Champaign, p. MS Thesis. 2006.

35. CHIN, S. T. **Numerical Investigation of the Effect of Wall-Wetting on Hydrocarbon Emissions in Engines**. M.Sc Thesis: University of Illinois. Urbana. 2001.

36. ZENG, Y. **Modeling of Multicomponent Fuel Vaporization in Internal Combustion Engines**. PhD Disseritation: University of Illinois. Urbana. 2000.

37. TORRES, D. J.; O'ROURKE, P. J.; AMSDEN, A. A. Efficient Multicomponent Fuel Algorithm. **Combustion Theory and Modelling (vol 7)**, p. 67–86, 2003.

38. TRUJILLO, M. F. **Spray and Single Droplet Impingement on a Wall**. PhD Disseritation: University of Illinois. Urbana. 2001.

APPENDIX A: SAMPLE INPUT FOR 12 SPECIES

Flag to trigger detchem.f

```
nsp       12   1 chemkin
```

Species Information table

```
c14h30   1.0      0.00001
    o2   mw2     31.99880   htf2      0.00000
    n2   mw3     28.01340   htf3      0.00000
   co2   mw4     44.00995   htf4    -93.99225
   h2o   mw5     18.01534   htf5    -57.76079
     h   mw6      1.00797   htf6     52.06081
    h2   mw7      2.01594   htf7      0.00000
     o   mw8     15.99940   htf8     59.51677
     n   mw9     14.00670   htf9    112.88000
    oh   mw10    17.00737   htf10     9.31119
    co   mw11    28.01055   htf11   -26.40088
    no   mw12    30.00610   htf12    21.56610
```

Molecular weights (gm/mol)

Heat of formation at 0 K (kcal/mol)

```
!------------ b r e a k (other input) -------
```

Species Composition Table

```
mfracfu,          0.000000
mfraco2,          0.232395
mfracn2,          0.767605
mfracco2,         0.000000
mfrach2o,         0.000000
mfrach,           0.000000
mfrach2,          0.000000
mfraco,           0.000000
mfracn,           0.000000
mfracoh,          0.000000
mfracco,          0.000000
mfracno,          0.000000
```

Initial mass fractions

```
!------------ b r e a k (other input) -------

 nrk        52
 nre        0
```

A dummy value which will be internally over-written

APPENDIX B: SAMPLE ENTHALPY INPUT FILE

```
                o2
                -1.998,  -1.348,  -0.678,   0.013,   0.724,
 1.457,          2.212,   2.988,   3.785,   4.600,   5.430,
 6.269,          7.116,   7.970,   8.832,   9.701,  10.576,
11.458,         12.346,  13.241,  14.141,  15.047,  15.958,
16.875,         17.797,  18.724,  19.656,  20.593,  21.534,
22.480,         23.430,  24.384,  25.343,  26.305,  27.272,
28.242,         29.217,  30.195,  31.176,  32.161,  33.150,
34.141,         35.136,  36.135,  37.136,  38.140,  39.147,
40.157,         41.169,  42.185,  43.202
154.77          5.01E+07   0.02

               n2
                -2.029,  -1.362,  -0.679,   0.013,   0.711,
 1.415,          2.129,   2.854,   3.596,   4.355,   5.131,
 5.920,          6.720,   7.531,   8.351,   9.179,  10.014,
10.856,         11.704,  12.557,  13.415,  14.277,  15.143,
16.012,         16.884,  17.759,  18.636,  19.515,  20.396,
21.278,         22.162,  23.048,  23.935,  24.823,  25.713,
26.604,         27.496,  28.389,  29.284,  30.180,  31.076,
31.974,         32.873,  33.774,  34.675,  35.577,  36.480,
37.384,         38.288,  39.193,  40.098
126.76          3.40E+07   0.04

              co2
                -2.067,  -1.523,  -0.818,   0.016,   0.957,
 1.984,          3.083,   4.242,   5.451,   6.703,   7.988,
 9.299,         10.632,  11.985,  13.356,  14.741,  16.141,
17.553,         18.976,  20.408,  21.849,  23.297,  24.751,
26.210,         27.675,  29.144,  30.617,  32.093,  33.573,
35.055,         36.540,  38.028,  39.518,  41.011,  42.506,
44.004,         45.504,  47.006,  48.512,  50.020,  51.530,
53.044,         54.559,  56.078,  57.598,  59.121,  60.645,
62.171,         63.699,  65.226,  66.754
304.21          7.37E+07   0.23

              h2o
                -2.227,  -1.523,  -0.771,   0.015,   0.827,
 1.660,          2.516,   3.396,   4.303,   5.241,   6.212,
 7.216,          8.249,   9.312,  10.401,  11.515,  12.652,
13.811,         14.989,  16.186,  17.400,  18.630,  19.875,
21.133,         22.404,  23.687,  24.981,  26.284,  27.597,
28.918,         30.248,  31.584,  32.928,  34.278,  35.634,
36.995,         38.362,  39.733,  41.110,  42.490,  43.875,
45.264,         46.656,  48.053,  49.452,  50.855,  52.262,
53.672,         55.084,  56.500,  57.918
134.45          3.51E+07   0.05
```

51 Enthalpy points from T = 0 to 5,000 K In kcal/mol

Critical temperature

Critical pressure

Acentric value (not explained in KIVA-4 Manual)

APPENDIX C: SAMPLE INPUT FOR 31 SPECIES

```
  nsp      31  1 chemkin
   c7h16  1.0     0.00001
!--- input for first 12 species goes here ---
!--- not pasted here to save paper ----------
     ho2  mw13   33.00677  htf13    2.49723
    h2o2  mw14   34.01474  htf14  -32.50716
    ch3o  mw15   31.03446  htf15    3.89386
    ch2o  mw16   30.02649  htf16  -27.68452
     hco  mw17   29.01852  htf17   10.39339
     ch2  mw18   14.02709  htf18   92.42695
     ch3  mw19   15.03506  htf19   34.79791
     ch4  mw20   16.04303  htf20  -17.88715
    c2h3  mw21   27.04621  htf21   68.36708
    c2h4  mw22   28.05418  htf22   12.53028
    c2h5  mw23   29.06215  htf23   27.99772
    c3h4  mw24   40.06533  htf24   45.59766
    c3h5  mw25   41.07330  htf25   40.36248
    c3h6  mw26   42.08127  htf26    4.64711
    c3h7  mw27   43.08924  htf27   24.00262
 c7h15-2  mw28   99.19760  htf28    1.29919
 c7h15o2  mw29  131.19640  htf29  -31.63032
 c7ket12  mw30  146.18783  htf30  -84.89719
 c5h11co  mw31   99.15397  htf31  -22.37608
!------------ b r e a k (other input) -------
!--- input for first 12 species goes here ---
!--- not pasted here to save paper ----------
 mfracho2,       0.000000E+00
 mfrach2o2,      0.000000E+00
 mfracch3o,      0.000000E+00
 mfracch2o,      0.000000E+00
 mfrachco,       0.000000E+00
 mfracch2,       0.000000E+00
 mfracch3,       0.000000E+00
 mfracch4,       0.000000E+00
 mfracc2h3,      0.000000E+00
 mfracc2h4,      0.000000E+00
 mfracc2h5,      0.000000E+00
 mfracc3h4,      0.000000E+00
 mfracc3h5,      0.000000E+00
 mfracc3h6,      0.000000E+00
 mfracc3h7,      0.000000E+00
 mfracc7h15-2,   0.000000E+00
 mfracc7h15o2,   0.000000E+00
 mfracc7ket12,   0.000000E+00
 mfracc5h11co,   0.000000E+00
!------------ b r e a k (other input) -------
  nrk       52
  nre       0
```